

1 **The Benefits of Continuous Local Regression for Quantifying Global Warming**

2

3 **David C. Clarke¹, Mark Richardson^{2,3}**

4

5 ¹Independent Researcher, Montreal, Quebec, Canada

6 ²Jet Propulsion Laboratory, California Institute of Technology, USA

7 ³Colorado State University, Fort Collins, USA

8

9 Corresponding author: David C. Clarke (davidcclarke.research@gmail.com)

10 **Key Points:**

- 11
- 12 • Continuous local regression is an alternative to traditional IPCC temperature change estimation methods.
 - 13 • Global warming, estimated from combined land and sea-surface temperature
 - 14 observational series with enhanced surface coverage, reached 1.14°C in 2019
 - 15 relative to 1850—1900 (likely range 1.05—1.25°C).
 - 16 • Global surface air temperature anomalies reached 1.21°C in 2019 relative to
 - 17 1850—1900 (1.11—1.32°C), implying a remaining carbon budget of ~220 GtCO₂
 - 18 to limit warming to 1.5°C.

19 **Abstract**

20 Change in global mean surface temperature (Δ GMST), based on a blend of land air and ocean
21 water temperatures, is a widely cited climate change indicator that informs the Paris Agreement
22 goal to limit global warming since preindustrial to “well below” 2°C. Assessment of current
23 Δ GMST enables determination of remaining target-consistent warming and therefore a relevant
24 remaining carbon budget. In recent IPCC reports, Δ GMST was estimated via linear regression or
25 differences between decade-plus period means. We propose non-linear continuous local
26 regression (LOESS) using ± 20 year windows to derive Δ GMST across all periods of interest.
27 Using the three observational GMST datasets with almost complete interpolated spatial coverage
28 since the 1950s, we evaluate 1850—1900 to 2019 Δ GMST as 1.14°C with a likely (17—83 %)
29 range of 1.05—1.25°C, based on combined statistical and observational uncertainty, compared
30 with linear regression of 1.05°C over 1880—2019. Performance tests in observational datasets
31 and two model large ensembles demonstrate that LOESS, like period mean differences, is
32 unbiased. However, LOESS also provides a statistical uncertainty estimate and gives warming
33 through 2019, rather than the 1850—1900 to 2010—2019 period mean difference centered at the
34 end of 2014. We derive historical global near-surface air temperature change (Δ GSAT), using a
35 subset of CMIP6 climate models to estimate the adjustment required to account for the difference
36 between ocean water and ocean air temperatures. We find Δ GSAT of 1.21°C (1.11—1.32°C) and
37 calculate remaining carbon budgets. We argue that continuous non-linear trend estimation offers
38 substantial advantages for assessment of long-term observational Δ GMST.

39 **1 Introduction**

40 Estimates of global mean surface temperature anomalies (GMST), derived from a combination
41 of near-surface air temperatures from land stations and sea surface temperatures over oceans,
42 have long been a staple of climate study. GMST and derived trends or changes, Δ GMST, have
43 featured prominently in IPCC reports, and are a key component in assessments of climate change
44 attribution (Bindoff et al., 2013), climate model validation (Flato et al., 2013), global carbon
45 budgets (Rogelj et al., 2018) and climate impacts (Hoegh-Guldberg et al., 2018). Perhaps most
46 importantly, the IPCC’s long-term Δ GMST estimate of 0.85°C, based on the 1880—2012 linear
47 trend, was a key scientific input to the Paris agreement to keep global surface temperature
48 change well below 2°C (IPCC, 2014; UNFCCC, 2015).

49
50 The IPCC Fifth Assessment Working Group I Report (IPCC WG1 AR5; Hartmann et al., 2013a)
51 used three GMST datasets: HadCRUT4 (Morice et al., 2012), NASA GISTEMP (Hansen et al.,
52 2010) and NOAA MLOST (Vose et al., 2010). While HadCRUT4 begins in 1850, the NOAA
53 and NASA datasets only begin in 1880, so the 1880—2012 ordinary least squares (OLS) linear
54 trend was presented as a “headline” warming estimate along with the HadCRUT4 1850—1900 to
55 2003—2012 difference in the Summary for Policymakers (IPCC, 2013). OLS trends for all
56 datasets were also given for 1951—2012 and 1979—2012 with uncertainties adjusted to account
57 for autocorrelated residuals (Santer et al., 2008; Hartmann et al., 2013b).

58
59 The IPCC Special Report on Global Warming of 1.5°C (IPCC SR1.5; Allen et al., 2018)
60 included two new GMST datasets that incorporated sophisticated spatial interpolation: Cowtan-
61 Way (Cowtan & Way, 2014a; Cowtan & Way, 2014b; Cowtan et al., 2015) and Berkeley Earth
62 (Rohde et al., 2013). Reported Δ GMST was 0.87 \pm 0.12°C based on the average of HadCRUT4,

63 NOAA, NASA and Cowtan-Way. An observation based estimate of Global Surface Air
64 Temperature change (Δ GSAT) was introduced by adjusting HadCRUT4 Δ GMST to account for
65 incomplete coverage and discrepancy in ocean air and sea-surface temperature anomalies, thus
66 producing an estimate of air near-surface temperature at 2 m over the entire globe (Rogelj et al.,
67 2018; Cowtan et al., 2015). The Δ GSAT estimate of 0.97°C in 2006—2015 implied lower
68 remaining carbon budgets compared to preceding studies based on Δ GMST consistent with
69 AR5's 0.85°C through 2012 (Millar et al., 2017a, 2017b; Goodwin et al., 2018; Richardson et al.,
70 2018).

71
72 IPCC WG1 AR5 Box 2.2 discusses the following issues with linear trends for estimating
73 Δ GMST: 1) poor approximation of trend evolution over time; 2) poor fit of residuals unamenable
74 to correction via autoregressive or moving average models; 3) high sensitivity to selected period;
75 and 4) divergent or even contradictory sub-period estimates relative to that of a larger
76 encompassing interval. The latter two issues were particularly relevant in AR5 Section 2.4.3's
77 discussion of the "observed reduction in warming trend" over 1998—2012 compared to 1951—
78 2012 (Rahmstorf et al., 2017; Risbey et al., 2018). A smoothing spline non-linear trend fit was
79 demonstrated to address these factors, and later studies presented alternative estimators for
80 continuous long-term Δ GMST trends (Cahill et al., 2015; Peng-Fei et al., 2014; Mudelsee, 2019;
81 Visser et al., 2018).

82
83 An issue of particular concern is that linear trends underestimate long-term (> 100 years)
84 Δ GMST compared to other estimates. For example, IPCC AR5 Box 2.2 estimated HadCRUT4
85 1900—2012 trends of $0.075 \pm 0.013^{\circ}\text{C decade}^{-1}$ and $0.081 \pm 0.010^{\circ}\text{C decade}^{-1}$ for linear OLS
86 and smoothing spline trends respectively. Generally, long-term linear fit Δ GMST from 1880 to
87 present is 0.05 — 0.10°C below nonlinear estimates (SR15 table 1.2; Visser et al., 2018) although
88 the spread in Δ GMST estimates between different datasets is commonly as wide as differences
89 engendered by Δ GMST methodology. Ultimately, IPCC AR5 Box 2.2 recommended linear
90 trends over non-linear estimates, noting that HadCRUT4 OLS-based long-term Δ GMST lay
91 within the 5-95% uncertainty range from the smoothing spline. Nevertheless, as the IPCC enters
92 the Sixth Assessment Report (AR6), a new method that supplements or supplants the traditional
93 approaches could reduce known biases and address these shortcomings.

94
95 This work proposes a local regression technique (LOESS, Cleveland et al., 1992; Cleveland,
96 1979) with a ± 20 year smoothing window for multi-decadal analysis. We also provide statistical
97 uncertainty and show that the fit residuals follow the assumed ARMA(1, 1) autocorrelation
98 structure. The framework can be extended to give self-consistent Δ GMST estimates with
99 uncertainty over as little as 15 years, providing a potential alternative to linear fits over all
100 intervals of interest.

101
102 However, here we focus on long-term Δ GMST and associated carbon budgets, directly relating
103 our estimates to approaches discussed in AR5 and SR1.5. We compare against the IPCC
104 approaches of OLS (1880—latest year) and period mean differences (from "preindustrial"
105 reference period 1850—1900 to the latest decade), as well as a global warming index which
106 SR1.5 used as the main estimate of "human-induced warming" (Haustein et al., 2017). We also
107 test the performance of our LOESS estimates using output from the two model large ensembles
108 with simulations that begin in 1850. Our final comparison is with the new CMIP6 model

109 ensemble, and using a subset of this ensemble we derive a modest conversion factor to update
110 our observation-based Δ GMST to Δ GSAT for carbon budget calculations.

111
112 The paper is structured as follows. Section 2.1 describes source data from observations and
113 associated estimated radiative forcings (2.1.1), two large model ensembles (2.1.2) and CMIP6
114 models (2.1.3). Section 2.2 describes trend estimation (2.2.1), evaluation of Δ GMST methods
115 and performance (2.2.2), large model ensemble evaluation (2.2.3) and Δ GSAT and carbon
116 budget calculation (2.2.4). We present our results in Section 3, covering long-term Δ GMST
117 analysis (3.1), large model ensemble analysis (3.2) and Δ GSAT and associated remaining carbon
118 budgets (3.3). Finally in Section 4 we discuss our results and issue recommendations for the use
119 of Δ GMST and Δ GSAT in future IPCC assessments.

120

121 **2 Source Data and Methods**

122 2.1.1 Global surface temperature datasets

123 Typically, gridded monthly land surface air temperature (LSAT) and sea surface temperature
124 (SST) anomalies are generated then blended to produce GMST. Table 1 summarizes five blended
125 LSAT-SST series in widespread use. There is considerable overlap in the underlying datasets.
126 There are two SST data sets: HadSST3 (Kennedy et al., 2011) and NOAA's ERSSTv5 (Huang et
127 al., 2017), and three LSAT datasets: GHCNv4 (Menne et al., 2019), CRUTEM4 (Jones et al.,
128 2010), and Berkeley Earth (Rohde et al., 2013). Even this understates the overlap; for example,
129 both SST datasets rely primarily on the comprehensive store of maritime observations from the
130 International Comprehensive Ocean-Atmosphere Data Set (ICOADS, Freeman et al., 2016),
131 albeit processed, filtered and supplemented in different ways. It is important to note, however,
132 that there are important differences between each group's quality assurance and data
133 homogenization procedures, and associated uncertainties, in both the land and SST datasets. In
134 particular, bias adjustments of SST data to account for differences between buoy, engine intake
135 and bucket measurements, can have a notable effect on long-term trends (Kennedy et al., 2019).

136

137 **Table 1.** Five operational observational datasets.

Series	Land (LSAT)	Ocean (SST)	Interpolation	Averaging	Start year
HadCRUT4 (Morice et al., 2012)	CRUTEM4	HadSST3	None	Simple average of hemispheric area-weighted averages	1850
NOAA GlobalTemp v5 (Zhang et al., 2019; Huang et al., 2020)	GHCNv4	ERSSTv5	Empirical orthogonal teleconnections (EOTs)	Area weighted average	1880
NASA GISTEMP v4 (Lenssen et al., 2019)	GHCNv4	ERSSTv5	Distance weighting (to 1200 km)	80 zones x 100 sub-boxes	1880
Cowtan-Way v2 (Cowtan & Way, 2014a; Cowtan & Way, 2014b; Cowtan et al., 2015)	CRUTEM4 (kriged)	HadSST3 (kriged)	Kriging (Complete)	Area weighted average	1850
Berkeley Earth (Rohde & Hausfather, 2020)	Berkeley Earth	HadSST3 (reprocessed & kriged)	Kriging (to ~2500 km)	Area weighted average	1850

138 Differences in spatial interpolation can affect calculated GMST. HadCRUT4 calculates area-
 139 weighted hemispheric means with no interpolation between its $5^{\circ} \times 5^{\circ}$ grid boxes, combined in a
 140 “simple” (equally-weighted) average. In contrast, NASA GISTEMP, Cowtan-Way and Berkeley
 141 Earth use extensive interpolation and, crucially, extrapolate LSAT over sea ice. Cowtan-Way
 142 interpolates HadCRUT4 to produce 100% apparent coverage, while GISTEMP and Berkeley
 143 Earth both interpolate up to 1200 km from observations, resulting in virtual areal coverage two to
 144 three times that of HadCRUT4 in the late 19th century. Nominal coverage in all three datasets is
 145 virtually complete since 1951 (see Figure S1, Supplementary Information). Reducing Cowtan-
 146 Way coverage to that of Berkeley Earth results in imperceptible differences in GMST even in the
 147 19th century, indicating that distance-limited and unlimited kriging interpolation can be
 148 considered equivalent (See Figure S14, Supplementary Information). Spatial smoothing via
 149 empirical orthogonal teleconnections (EOTs; van den Dool et al., 2000) in NOAA GlobalTemp
 150 (and ERSSTv5) results in nominal coverage between that of HadCRUT4 and NASA GISTEMP,
 151 but largely misses very high latitudes and has no interpolated coverage over Arctic sea ice.

152 Comparisons with temperature reanalyses, independent surface data and satellite retrievals show
 153 that interpolation significantly mitigates coverage bias (and associated underestimation of
 154 warming) arising from poor sampling of the fastest warming areas, especially the Arctic, since

155 the mid-twentieth century (Dodd et al., 2015; Cowtan et al., 2018a; Susskind et al., 2019;
 156 Lennsen et al., 2019). Evidence is mixed for earlier periods where reduced coverage leads to
 157 larger interpolation uncertainty (Cowtan et al., 2018a) and differences between underlying SST
 158 datasets are the largest source of discrepancies. Cowtan et al. (2018a) showed that both
 159 generalized least squares averaging and kriging interpolation mitigated errors engendered by
 160 “naïve” global or hemispheric averaging methods, such as those used in HadCRUT4, which
 161 implicitly set “missing” areas to the global average of sampled areas (Hansen et al., 2006). Thus,
 162 the three interpolated datasets are demonstrably more representative of global climate change.

163 We use the published monthly anomaly series, except for Berkeley Earth where we use the area-
 164 weighted average of the gridded series, which diverges from the published series over 1850—
 165 1950 (Supplementary Information, Figures S2, S3). For series starting in 1850 anomalies are
 166 relative to 1850—1900 while NASA GISTEMP and NOAA GlobalTemp are baselined such that
 167 their 1880—1900 mean matches that of the three longer-running datasets. These rebaselined
 168 NASA and NOAA series are used for all ΔGMST estimates calculated relative to 1850—1900 as
 169 outlined in Section 2.2.1. This streamlined and consistent scheme replaces multiple IPCC SR1.5
 170 approaches based on scaling their 1880—2015 trends or matching to HadCRUT4 over 1880—
 171 1990. We also report the mean ΔGMST for all five operational datasets (OpAll group) and the
 172 subset of three datasets with near-global interpolated coverage post-1950 (Global_3 group), with
 173 the latter used as the basis for our main estimates. Group ΔGMST estimates are the mean of the
 174 individual estimates as in IPCC AR5.

175 We augment temperature data with summarized anthropogenic and natural radiative forcing data
 176 required to derive the “global warming index” referenced in SR1.5 as a potential alternative to
 177 ΔGMST for tracking anthropogenic warming (Haustein et al., 2017; Allen et al., 2018). These
 178 are used to estimate anthropogenic and natural forced changes, $\Delta\text{GMST}_{\text{F,anthro}}$ and $\Delta\text{GMST}_{\text{F,nat}}$,
 179 using a two-box impulse-response model with parameters derived from a least-squares-fit
 180 between observed temperatures and the modelled response (Otto et al., 2015; Haustein et al.,
 181 2017). These estimates are used to assess the characteristics of a particular LOESS window
 182 choice (Section 2.2.1) and as an additional comparator to long-term ΔGMST .

183 2.1.2 Model Large Ensembles

184 We perform tests using output from the large ensembles whose simulations begin in 1850: the
 185 Max Planck Institute for Meteorology Grand Ensemble (MPI-GE, N=100, Maher et al., 2019)
 186 and Commonwealth Scientific and Industrial Research Organisation Mk3.6.0 (CSIRO Mk3.6.0,
 187 N=30, Rotstayn et al., 2012; Jeffrey et al., 2013), taking their GSAT over historical-RCP8.5
 188 simulations for 1850—2019 and baselining each to 1850—1900. We exclude five other large
 189 ensembles that start after 1850 (Deser et al, 2020), and our approach is conceptually similar to
 190 that in Dessler et al. (2018)’s estimation of how internal variability affects derived climate
 191 sensitivity in MPI-GE. The use of GSAT simplifies the calculations and since the year-to-year
 192 variability in GSAT-GMST difference is of order 0.01 °C in CMIP5 models (e.g. Figure 2 of
 193 Cowtan et al. 2015), we expect little effect of blending or masking on this particular analysis.

194
 195 Conceptually, we first decompose ΔGSAT as:

$$196 \quad \Delta\text{GSAT}_{\text{total}} = \Delta\text{GSAT}_{\text{F}} + \Delta\text{GSAT}_{\text{var}} \quad (1)$$

197 where $\Delta\text{GSAT}_{\text{var}}$ represents internal variability and $\Delta\text{GSAT}_{\text{F}}$ the forced response. The same
 198 decomposition would apply for ΔGMST . We adopt the IPCC SR1.5 argument that “[s]ince 2000,
 199 the estimated level of human-induced warming has been equal to the level of observed warming
 200 with a *likely* range of $\pm 20\%$ ”. From this it follows that a reliable estimate of $\Delta\text{GMST}_{\text{F}}$ through
 201 2019 would be an appropriate estimate of human-induced warming, $\Delta\text{GMST}_{\text{F,anthro}}$, with
 202 relevance for temperature targets and carbon budgets. With just one realization of real-world
 203 internal variability we cannot perform this decomposition, but a large ensemble mean should
 204 approach that model’s $\Delta\text{GMST}_{\text{F}}$. We test whether our derived $\Delta\text{GMST}_{\text{LOESS}}$ approximates
 205 $\Delta\text{GMST}_{\text{F}}$, and consider the decomposition in an individual run to be:

$$206 \quad \Delta\text{GMST}_{\text{total}} = \Delta\text{GMST}_{\text{LOESS}} + \Delta\text{GMST}_{\text{resid}} \quad (2)$$

207 With a ± 20 -year window this effectively decomposes between short- and long-term ΔGMST . If
 208 periods are selected to minimize volcanism (which induces short-term $\Delta\text{GMST}_{\text{F}}$), and the
 209 magnitude of $\Delta\text{GMST}_{\text{var}}$ is small at 40-year timescales, then resultant $\Delta\text{GMST}_{\text{LOESS}} \approx$
 210 $\Delta\text{GMST}_{\text{F,anthro}}$ over the long-term intervals of interest.

211 2.1.3 Coupled Model Intercomparison Project, phase 6 (CMIP6) output

212 We include historical simulations over 1850—2014 from CMIP6 models which have the
 213 required fields for blending surface air temperatures (SAT) over land or sea ice and SST over
 214 ocean (Eyring et al, 2016), permitting “apples-to-apples” comparisons with land-ocean
 215 observational datasets and derivation of a $\Delta\text{GMST}_{\text{LOESS}}$ to $\Delta\text{GSAT}_{\text{LOESS}}$ adjustment. These
 216 include near-surface air temperature (“tas”), sea surface temperature (“tos”) and sea ice
 217 concentration (“siconc” or “siconca”, N=24 simulations listed in Table S1).

218 Following Cowtan et al (2015) and Richardson et al (2018), each simulation is processed to
 219 produce two area-weighted average series: 1) global SAT (i.e. GSAT) and 2) global blended
 220 SAT-SST (i.e. GMST). At each grid cell i, j , the blended monthly temperature $T_{\text{blend},i,j}$ is:

$$221 \quad T_{\text{blend},i,j} = w_{\text{SAT},i,j} T_{\text{SAT},i,j} + (1 - w_{\text{SAT},i,j}) T_{\text{SST},i,j} \quad (3)$$

222 where $w_{\text{SAT},i,j}$ is the land plus sea ice grid cell fraction, and $T_{\text{SAT},i,j}$ and $T_{\text{SST},i,j}$ are the local
 223 anomalies relative to 1850—1900. For GSAT $w_{\text{SAT},i,j} = 1$ everywhere, and for the blended GMST
 224 series $w_{\text{SAT},i,j} = 1$ in ocean cells for a calendar month if any those months during 1961-2014 has
 225 siconc $> 1\%$. This is similar to the Cowtan-Way blending algorithm and the “xaf” simulations in
 226 Cowtan et al. (2015).

227 2.2 Methods

228 Next we describe our approach to obtain ΔGMST , our uncertainty estimation, and the remaining
 229 carbon budget calculation. Section 2.2.1 explains the trend fits and errors; Section 2.2.2 explains
 230 the ΔGMST calculations, observational error and methods by which the fit quality are judged
 231 using observational data. Section 2.2.3 discusses the large ensemble methodology, and Section
 232 2.2.4 the CMIP6 comparison and carbon budget calculation. We use ΔGMST and ΔGSAT to
 233 refer to a general change in global temperature, and use qualifiers or subscripts when referring to
 234 statistical estimation methods or its components. For example, $\text{LOESS}_{\text{bsln}} \Delta\text{GMST}$ (or

235 $\Delta\text{GMST}_{\text{LOESS}}$) refers to an estimate made with LOESS, while $\Delta\text{GMST}_{\text{F}}$ refers to the forced
 236 component.

237 2.2.1 Trend calculations and their statistical uncertainty

238 For a series of n temperature observations x_i at time t_i , a linear trend is:

239
$$x_i = a + bt_i + e_i, i = 1, \dots, n \quad (4)$$

240 where a and b are intercept and slope parameters to be fitted and e_i are residual errors. The slope
 241 estimate \hat{b} is used to obtain ΔGMST as $\hat{b}(t_n - t_i)$, with the uncertainty of \hat{b} (and thus ΔGMST)
 242 determined as explained below.

243 Our multi-decadal LOESS point-to-point (LOESS_{md}) ΔGMST is based on the LOESS fit from
 244 1880—2019; for any starting point, ΔGMST to 2019 is the LOESS_{md} fit evaluated in 2019 minus
 245 the start value. We also introduce “baseline” LOESS ($\text{LOESS}_{\text{bsln}}$) as our main ΔGMST estimate.
 246 $\text{LOESS}_{\text{bsln}}$ is simply the same fit evaluated at the end year, yielding an estimate relative to
 247 1850—1900 baseline, rather than to a given start year such as 1880. Although the central
 248 estimated fit is the same, the associated statistical fit uncertainties are quite different, as
 249 explained below.

250 Our LOESS_{md} uses a fixed span α_{md} of ± 20 years, tricube weighting (the default) and a degree 1
 251 smoothing parameter (i.e. locally weighted linear trend, which yields more stable end points).
 252 Tests with the Cowtan-Way series show that α of ± 10 years captures internal decadal variability
 253 and has marked sensitivity to volcanic episodes early in the record and to a lesser extent over
 254 1980—2019 (Figure S4). On the other hand, α of ± 20 or ± 30 years smooth out short-term
 255 variability and show similar warming from 1850—1900 to present: 1.12°C (± 20 years) or 1.11°C
 256 (± 30 years). Analysis of first differences for each LOESS window (Figures S5) shows large
 257 variance with α of ± 5 years, which stabilises with α of ± 20 , ± 25 or ± 30 years. Large ensemble
 258 tests support this choice: α_{md} substantially smaller than ± 20 years increases $\Delta\text{GMST}_{\text{F}}$
 259 discrepancy, while substantially longer than ± 20 years introduces a low bias in 1850—2019
 260 ΔGMST (Figures S6, S7). We therefore choose $\alpha_{\text{md}} = \pm 20$ years to evaluate trends of length ≥ 30
 261 years; $\text{LOESS}_{\text{pent}}$ ($\alpha = \pm 5$ years) is reserved for future extension of our framework to cover very
 262 short-term trends of ≤ 15 years (see Figure S4, panel d).

263 Default methods assume statistically independent noise, necessitating an uncertainty correction if
 264 the fit residuals are autocorrelated. Santer et al (2000) presented a procedure for assessing an
 265 effective sample size (and associated reduction in degrees of freedom) from the general formula

266
$$n_e = \frac{n_t}{(1 + 2 \sum_{j=1}^{n-1} \rho_j)} \quad (5)$$

267 where ρ_j is the autocorrelation function of a noise model estimated from the fit residuals. If the
 268 noise follows an autoregressive(1) (AR(1)) process, then with $\rho_j = \phi^j$
 269

270
$$1 + 2 \sum_{j=1}^{n-1} \rho_j \approx 1 + \frac{2\phi}{(1-\phi)} = \frac{(1+\phi)}{(1-\phi)} \quad (6)$$

271 where ϕ is estimated from the lag-one autocorrelation coefficient (Mitchell et al, 1966).
 272 However, Foster and Rahmstorf (2011) demonstrated that 1979-2010 GMST trend residuals
 273 were more consistent with an autoregressive moving average, ARMA(1, 1) model in the form

274
$$\rho_1 = \frac{(\phi + \theta)(1 + \phi\theta)}{1 + 2\phi\theta + \theta^2} \quad (7)$$

$$\rho_j = \rho_1 \phi^{j-1} \quad j \geq 2$$

275 Substituting (6) into (5) yields

276
$$1 + 2 \sum_{j=1}^{n-1} \rho_j \approx 1 + \frac{2\rho_1}{(1-\phi)} \quad (8)$$

277 Foster and Rahmstorf used the Yule-Walker “method of moments” with $\hat{\phi} = \hat{\rho}_1 / \hat{\rho}_2$. Hausfather
 278 et al. (2017) instead used Maximum Likelihood Estimation (MLE) to obtain $\hat{\phi}$ and $\hat{\theta}$ and then $\hat{\rho}_1$
 279 via Eq. (6). Monte Carlo simulations show that MLE gives a more robust and efficient estimator
 280 $\hat{\phi}$, suitable for series as short as 8 years (see Figure S8). Hausfather et al. also introduced a bias
 281 correction to account for underestimated autocorrelation in shorter series, derived from AR(1) in
 282 Tjøstheim and Paulsen (1996) and extended to account for the positive difference between $\hat{\phi}$ and
 283 $\hat{\rho}_1$.

284
$$\hat{\phi}_{BC} = \hat{\phi} + \left(1 + 4(2\hat{\phi} - \rho_1)\right) / n_t \quad (9)$$

$$\rho_{1BC} = \rho_1 + \left(1 + 4(2\hat{\phi} - \rho_1)\right) / n_t$$

285 Although this bias correction is most pertinent for very short series, Monte Carlo simulations
 286 have demonstrated its relevance for highly autocorrelated series up to 720 months in length. We
 287 selected this bias correction after comparison with alternatives (e.g. Nychka et al., 2000; see
 288 Figure S9).

289 Substituting the bias corrected parameters and simplifying the correction term as in (5) yields the
 290 final effective length correction.

291
$$n_e = \frac{n_t}{1 + 2 \sum_{j=1}^{n-1} \rho_j} \approx \frac{n_t}{1 + 2\rho_{1BC} / (1 - \hat{\phi})} \quad (10)$$

292 We estimate corrections from the residuals of both LOESS and OLS. To apply this correction,
 293 we define nominal degrees of freedom $\nu = n_t - p$ and effective degrees of freedom $\nu_e = n_e - p$,
 294 where p is the number of actual or equivalent parameters of the trend fitting methodology.

295 In the linear case, the correction is applied directly to s_b , the standard error of b in (1), with $p = 2$.

$$296 \quad s'_b = s_b \frac{v}{v_e} = s_b \sqrt{\frac{n_t - 2}{n_e - 2}} \quad (11)$$

297 For non-parametric trend estimation like LOESS, Monte Carlo simulations can establish
 298 uncertainties, as in Visser et al (2016) for smoothing spline trends. Here we propose a plausible
 299 heuristic method. First the above correction is applied to s_e , the standard errors of the residual fit,
 300 with p set to the equivalent number of parameters of the LOESS trend, derived from the trace of
 301 the LOESS projection matrix (Cleveland and Grosse, 1991); generally $p \approx 2/\alpha + 0.5$ for GMST
 302 datasets. For an equally spaced time series, s_e is maximum at the start and end of the LOESS fit.
 303 If statistical errors at these two points are independent, they may be combined in quadrature, by
 304 taking the square root of the sum of the squared standard errors, i.e. the square root of the sum of
 305 variances (see also Eq S4 in Karl et al., 2015). Then the corrected standard error $s'_{\Delta T_n}$ for
 306 ΔGMST_n becomes

$$307 \quad s'_{\Delta T_n} = \sqrt{2} \max(s'_e) = \sqrt{2} \max(s_e) \sqrt{\frac{n_t - p}{n_e - p}} \quad (12)$$

308 For both OLS and LOESS_{md} we evaluate the sample autocorrelation function (ACF) of the fit
 309 residuals as well as the ACFs of the ARMA(1, 1) and AR(1) noise models fit to those residuals.

310 Finally, for LOESS_{bsln} we assume that the mean error during the 1850—1900 baseline is small
 311 relative to the end point error. We are not aware of any formal method for calculating the
 312 required adjustment, so we generate an *ad hoc* correction tuned to perform well in Monte Carlo
 313 tests. To approximate the baseline uncertainty, we take the LOESS_{md} start point uncertainty,
 314 $\max(s'_e)$, and reduce it according to the relative length of the baseline by applying an appropriate
 315 factor b_{adj} . This is similar in principle to the reduction of sample mean uncertainty with
 316 increasing sample size; in this case, b_{adj} is tuned to reproduce the results of Monte Carlo tests
 317 with Cowtan-Way data. For a baseline t_1 to t_b , with $b \leq n/2$, where n is the length of the full
 318 series we take (while also imposing a lower limit on b_{adj}):

$$319 \quad b_{adj} = (t_{n/2} - t_b) / (t_{n/2} - t_1) ; 0.5 \leq b_{adj} \leq 1 \quad (13)$$

320 Following quadrature the combined LOESS_{bsln} error is then:

$$321 \quad s'_{\Delta T_n} = \sqrt{(b_{adj}^2 + 1)} \max(s'_e) = \sqrt{(b_{adj}^2 + 1)} \max(s_e) \sqrt{\frac{n_t - p}{n_e - p}} \quad (14)$$

322 and (12) is a special case of (14) with a baseline of length 0 and $b_{adj} = 1$. Monte Carlo
 323 simulations of LOESS fits plus ARMA(1, 1) noise produce a probability distribution function
 324 nearly identical to that engendered in Cowtan-Way by (12) over 1880—2019 and by (14) from
 325 1850—1900 and 1880—1900 to 2019 (Figures S10 and S11).

326 2.2.2 Estimates of observational Δ GMST, error components and performance tests

327 The main analysis focuses on long-term Δ GMST (results for other IPCC AR5 periods are in the
 328 Supplementary Information Table S2). In addition to OLS and LOESS_{md} Δ GMST over 1880—
 329 2019, and LOESS_{bsln} from 1850—1900 to 2019, we also calculate period difference Δ GMST
 330 estimates by subtracting mean GMST over 1850—1900 from the most recent decade, 2010—
 331 2019. The above are also compared to GMST-derived estimates of anthropogenic warming
 332 (Haustein et al., 2017; section 2.1.2) and to a CMIP6 ensemble (Section 2.2.4). Global_3 and
 333 OpAll group Δ GMST are the mean of individual dataset Δ GMST.

334 Following standard IPCC practice, we report the 5—95% statistical uncertainty range for LOESS
 335 and OLS Δ GMST estimates, as outlined in Section 2.2.1. Group uncertainties are reported
 336 conservatively and go from the smallest 5% to the largest 95% reported for any of their
 337 constituent datasets. We also report observational parametric uncertainty as the 5—95 % range
 338 of Δ GMST values derived from each of the 100-member HadCRUT4 and Cowtan-Way
 339 ensembles. These ensembles use a Monte-Carlo method to assess the fully correlated errors
 340 engendered by parametric uncertainty related to bias adjustments to individual temperature
 341 readings (Kennedy et al., 2011).

342 Figure S12 depicts these estimates and derived autocorrelation functions (ACF) for the Cowtan-
 343 Way monthly series with ARMA(1, 1) correction and for Cowtan-Way annual series with AR(1)
 344 correction (similar to IPCC AR5).

345 Finally we assess LOESS_{bsln} Δ GMST against period mean differences for the Global_3 group by
 346 evaluating at the mid-point of the corresponding end decade; for example, LOESS_{bsln} at the end
 347 of 2014 is comparable to the 1850—1900 to 2010—2019 period Δ GMST. IPCC SR1.5 explicitly
 348 considered their 1850—1900 to 2006—2015 Δ GMST estimate to be a proxy of the eventual
 349 1996-2025 mean. We therefore compare the Δ GMST estimates for every year from 1995 against
 350 centered 20-year and 30-year means. We also compare to “extended” running 30-year periods,
 351 generated by assuming a continuation of the 1990—2019 linear trend through 2029. We argue
 352 that a smaller bias and root mean square error (RMSE) relative to the 20- and 30-year means
 353 represents better performance according to the IPCC’s own criterion.

354 2.2.3 Large Ensemble Analysis for Method Validation and Uncertainty Calculation

355 LOESS_{bsln} is fit to the 1850—2019 annual output for each simulation, then the Δ GMST_{LOESS}
 356 through 2019 is evaluated from all start years 1850—1980. Separate linear OLS fits ending in
 357 2019 are also obtained for those start years. We also evaluate LOESS_{bsln} at the end of 2014 and
 358 compare with the 1850—1900 to 2010—2019 period Δ GMST (which we henceforth refer to as
 359 Δ GMST_{period}). Finally, LOESS_{md} is calculated over 1880—2019 for each simulation. The
 360 distribution of ensemble member Δ GMST- Δ GMST_F provides an estimate of the bias and
 361 uncertainties for each estimator and each period, as argued in Section 3.2. If
 362 Δ GMST<sub>LOESS} \approx \DeltaGMST_F then the LOESS residuals will be dominated by internal variability and
 363 our statistical uncertainty is related to error due to internal variability (we confirmed that the
 364 model residuals generally follow our assumed ARMA(1,1), Figure S13). The LOESS
 365 decomposition filters in time: Δ GMST_F excursions shorter than our window will inflate</sub>

366 statistical uncertainty, while multi-decadal $\Delta\text{GMST}_{\text{var}}$ changes will be included in $\Delta\text{GMST}_{\text{LOESS}}$
 367 and result in too small errors. We compare each run’s statistical uncertainties with the ensemble
 368 17—83 % and 5—95 % ranges to check for evidence that the observation-derived statistical
 369 uncertainties could represent internal variability in the 1850—1900 to 2019 $\Delta\text{GMST}_{\text{LOESS}}$ used
 370 for carbon budget calculations (see Section 2.2.4).

371 2.2.4 CMIP6 comparisons, GSAT adjustment and remaining carbon budget

372 IPCC SR15 reported remaining carbon budgets accounting for warming to date, but did not
 373 directly use the reported $\Delta\text{GMST}_{\text{period}}$ 5—95 % observational uncertainty from individual
 374 datasets. Instead AR5 5—95 % observational uncertainty through 1986-2005 was combined with
 375 additional uncertainties to produce a “likely” 17—83 % ΔGMST total uncertainty, and
 376 $\Delta\text{GMST}_{\text{period}}$ was then converted to $\Delta\text{GSAT}_{\text{period}}$ using a CMIP5-derived scaling. This Section
 377 describes the comparison with CMIP6 $\Delta\text{GMST}_{\text{period}}$ and conversion of observed $\text{LOESS}_{\text{bsln}}$
 378 ΔGMST to ΔGSAT , and then details the carbon budget calculation, which largely follows the
 379 IPCC SR1.5 methodology, as elaborated by Rogelj et al. (2019).

380 $\text{LOESS}_{\text{bsln}}$ series are generated for each of the 24 individual full-coverage CMIP6 air-only
 381 (GSAT) and blended (GMST) series described in Section 2.1.3, with the blended series being
 382 comparable to quasi-global GMST observations. We consider the full ensemble and also a sub
 383 ensemble of “likely ECS” models, excluding those with effective climate sensitivity (ECS)
 384 outside the CMIP5 1.9-4.5°C 90% ensemble range (Flato et al., 2013; Forster et al., 2019).

385 For each ensemble member’s $\text{LOESS}_{\text{bsln}}$ changes we derive a “blending” factor $A_{\text{blend}} =$
 386 $\Delta\text{GSAT}_{\text{LOESS}} / \Delta\text{GMST}_{\text{LOESS}}$, which represents the required adjustment to convert $\Delta\text{GMST}_{\text{LOESS}}$
 387 to $\Delta\text{GSAT}_{\text{LOESS}}$, accounting for the difference between GSAT air temperatures and GMST
 388 “blending” of air and water temperatures. The median and ensemble distribution of A_{blend} scaling
 389 factors is applied to observed $\Delta\text{GMST}_{\text{LOESS}}$ to obtain historical observed $\Delta\text{GSAT}_{\text{LOESS}}$ with
 390 combined uncertainty for calculating the remaining carbon budget, as detailed below. The carbon
 391 budget calculation largely follows the framework established in IPCC SR1.5 (Rogelj et al.,
 392 2017), elaborated by Rogelj et al (2019) and implemented by Nauel et al (2019). We simplify the
 393 Rogelj et al (2019) remaining carbon budget equation to:

$$394 \quad B_{\text{lim}} = \left(\Delta\text{GSAT}_{\text{lim}} - \Delta\text{GSAT}_{F,\text{anthro}} - \Delta\text{GSAT}_{\text{nonCO}_2,\text{fut}} \right) / \text{TCRE} - E_{\text{Esfb}} \quad (15)$$

395 where B_{lim} is the remaining carbon budget associated with a temperature limit $\Delta\text{GSAT}_{\text{lim}}$ (1.5 or
 396 2°C), with $\Delta\text{GSAT}_{F,\text{anthro}}$ (also referred to as $\Delta\text{GSAT}_{\text{hist}}$) the historical human-induced warming to
 397 date and $\Delta\text{GSAT}_{\text{nonCO}_2,\text{fut}}$ the expected future warming from non-CO₂ anthropogenic forcing.

398 TCRE is the transient climate response to cumulative CO₂ emissions, while E_{Esfb} is an
 399 adjustment for Earth system feedbacks from permafrost thaw and warming wetlands. This is
 400 essentially the same framework as SR1.5, except that in SR1.5 non-CO₂ warming was not
 401 separate, but rather included in TCRE, and the earth-system feedback adjustment was
 402 incorporated in the results of SR1.5 Table 2.2, but not included in “headline” estimates in its
 403 Summary for Policymakers (IPCC, 2018).

404 In practice, observations based $\Delta\text{GSAT}_{\text{obs}}$ (whether $\Delta\text{GSAT}_{\text{period}}$, $\Delta\text{GSAT}_{\text{LOESS}}$ or using another
 405 statistical technique) is used as an approximation of $\Delta\text{GSAT}_{\text{F,anthro}}$, following from the finding
 406 that observed and “human-induced” warming to date are approximately equivalent (Allen et al.,
 407 2018; Haustein et al., 2017). Thus, SR15 assessed $\Delta\text{GSAT}_{\text{F,anthro}}$ as 0.97°C in 2006-2015 relative
 408 to 1850—1900, based on the HadCRUT4 average for that decade (0.84°C) adjusted by the ratio
 409 between the equivalent CMIP5 blended-masked estimate (0.86°C) and CMIP 5 ΔGSAT
 410 (0.99°C), as stated in Box 2 of Rogelj et al. (2019).

411 Here we select the Global_3 GMST group and so do not need to rely on a model correction for
 412 the additional bias introduced by HadCRUT4’s incomplete and changing geographic coverage,
 413 which necessitates a correction substantially larger than A_{blend} . Our central estimate for
 414 $\Delta\text{GSAT}_{\text{F,anthro}}$ is:

$$415 \quad \Delta\text{GSAT}_{\text{F,anthro}} = A_{\text{blend_med}}\Delta\text{GMST}_{\text{Global_3}} \quad (16)$$

416 where $A_{\text{blend_med}}$ is the median value from CMIP6 A_{blend} ensemble and $\Delta\text{GMST}_{\text{Global_3}}$ is the
 417 LOESS_{bsln} ΔGMST of the Global_3 group (based on the mean of LOESS_{bsln} applied to each of
 418 the three series). It should be noted this is a very conservative adjustment, as it may not fully
 419 account for coverage bias in the early part of the instrumental record, and ignores the “ice edge
 420 effect” cooling bias introduced by the variable sea ice mask in NASA GISTEMP and Berkeley
 421 Earth, which would add an additional ~3% (Cowtan et al., 2015; Richardson et al., 2018).

422 SR1.5’s likely total uncertainty in $\Delta\text{GMST}_{\text{obs}}$ (and derived ΔGSAT) was $\pm 0.12^{\circ}\text{C}$. Here we
 423 derive likely observation-based $\Delta\text{GSAT}_{\text{LOESS}}$ using Gaussian approximations to the
 424 observational, dataset spread and statistical fit uncertainties in the following steps (tests and
 425 details in Supplementary Table S3):

- 426 1. The Cowtan-Way ensemble spread is our best estimate of observational parametric
 427 ΔGMST uncertainty, so for each dataset its standard deviation is combined in quadrature
 428 separately with (i) the dataset-specific statistical 1σ uncertainty and (ii) the CSIRO
 429 Mk3.6.0 large ensemble standard deviation.
- 430 2. For ΔGSAT , the CMIP6 A_{blend} ensemble standard deviation is taken as the uncertainty
 431 value, and combined in quadrature with the results of 1.
- 432 3. We estimate a 17—83 % range by calculating those percentiles for each dataset following
 433 a Gaussian assumption, i.e. $\pm 0.954\sigma$ from the mean, and then selecting the lowest 17 %
 434 and higher 83 % value from across the datasets.

435 There is no universally accepted method of accounting for dataset spread. We adopt step 3 as a
 436 conservative approach, however, by reporting the separate dataset uncertainties as described in
 437 Section 2.2.2 other groups can replicate or develop alternative uncertainty estimates.

438 We take Rogelj et al. (2019)’s, T_{nonCO_2} of 0.1°C (0.2°C) for T_{lim} of 1.5°C (2°C), and E_{Esfb} of 100
 439 Gt CO_2 through 2100. TCRE percentiles are based on AR5’s likely range of $0.2\text{--}0.7^{\circ}\text{C}$ per 1,000
 440 Gt CO_2 (Collins et al., 2013), as in Nauels et al (2019). SR1.5 included alternative carbon
 441 budgets using a lower T_{hist} from the average of the blended GMST datasets with no GSAT

442 adjustment. Our alternative uses the Global_3 average without the GSAT adjustment. To
443 contextualize the remaining budget against cumulative emissions to date we include data and
444 uncertainties from the 2019 Global Carbon Budget (Friedlingstein et al., 2019).

445 **3 Results**

446 3.1 Long term Δ GMST analysis

447 Figure 1 compares LOESS_{md} and OLS Δ GMST from 1880—2019 with associated 5—95%
448 uncertainties (Fig. 1a). Figure 1b shows that the LOESS fit residuals follow our assumed
449 ARMA(1, 1), which is necessary to justify our error correction and is not true for OLS (Figure
450 1c). Our full set of observational long-term Δ GMST estimates are given in Table 2.

451 Δ GMST_{OLS} is always lower than Δ GMST_{LOESS}, with some central OLS Δ GMST estimates lying
452 below the LOESS uncertainty range or nearly so (Cowtan-Way, Berkeley Earth). Datasets are
453 similarly ranked for both OLS and LOESS_{md} over 1880—2019, from HadCRUT4 (0.96, 0.99) to
454 Berkeley Earth (1.05, 1.14). The Global_3 interpolated series exhibit a greater relative difference
455 than the non-global series; the Berkeley Earth and HadCRUT4 LOESS_{md} difference is 0.21°C,
456 but only 0.13°C for OLS. Thus OLS not only renders lower Δ GMST, but also de-emphasizes the
457 differences between the datasets.

458

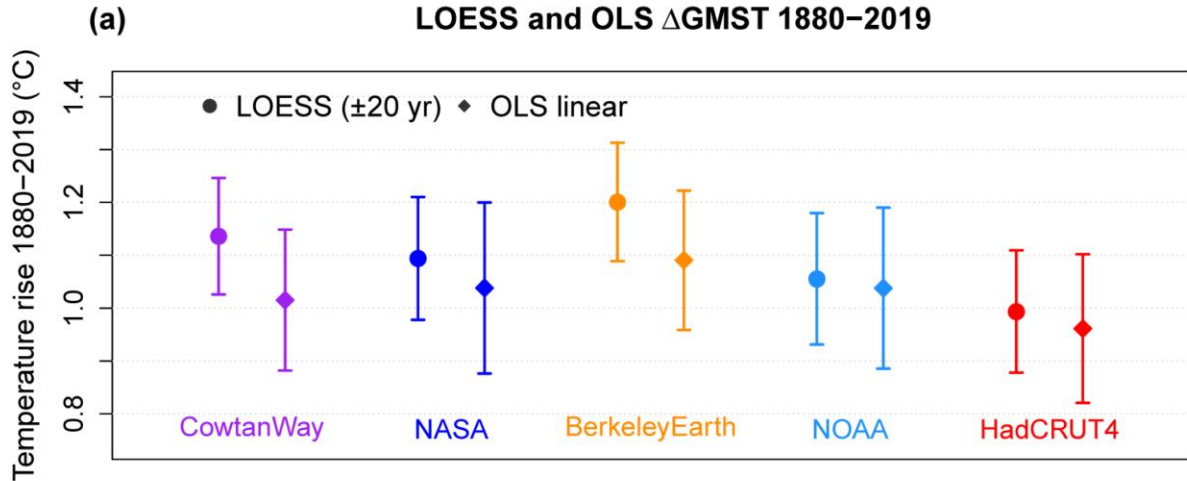
459

460

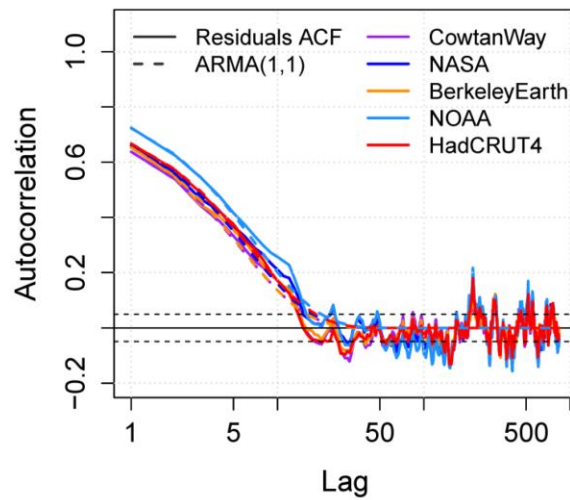
461

462

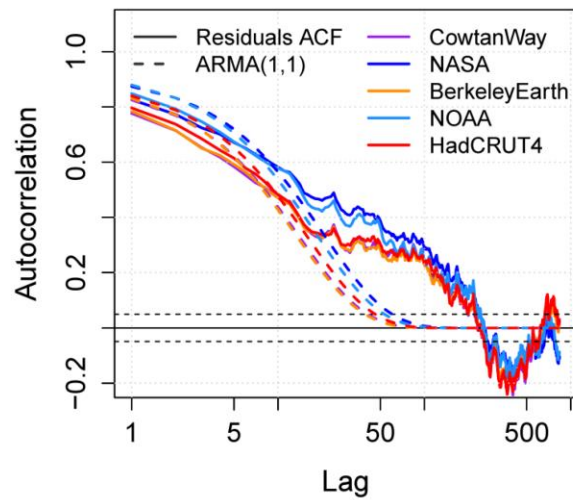
463



(b) **LOESS series residuals ACF**



(c) **OLS series residuals ACF**



464
 465 **Figure 1: 1880-2019 warming estimates from five GMST series.** (a) LOESS (span \pm 20 years) and OLS trends
 466 with 5-95% statistical fit uncertainty are shown for Cowtan -Way (purple), NASA GISTEMP (blue), Berkeley Earth
 467 (orange), NOAA GlobalTemp (light blue) and HadCRUT4 (red) over 1880-2019. (b) The autocorrelation function
 468 (ACF) of the LOESS fit residuals are shown for each series (solid lines), along with the ACF of the estimated
 469 ARMA(1, 1) model used to correct for autocorrelation. (c) As in (b) except for OLS linear trend.

470
 471

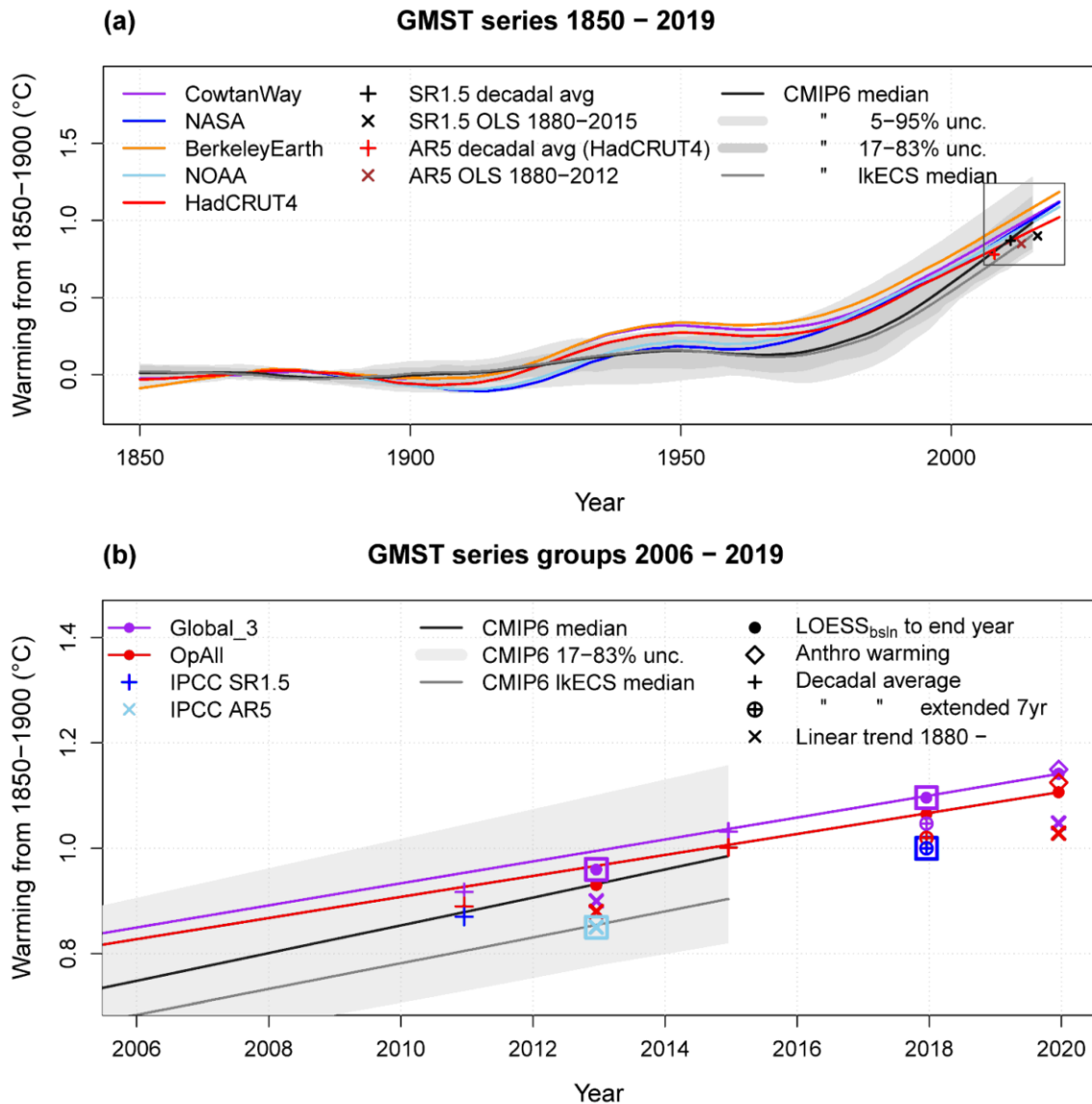
472

473

474 **Table 2: Observed increase in GMST (°C) in datasets and dataset groupings.** Numbers in square
 475 brackets correspond to 5–95% statistical fit uncertainty ranges, accounting for autocorrelation in fit
 476 residuals. Round brackets denote observational parametric uncertainty where available (HadCRUT4,
 477 Cowtan-Way). NOAA and NASA are each aligned to match 1880—1900 mean of the other three
 478 datasets. Best estimates from three full global series are denoted by *. Group mean estimates (in bold) are
 479 given with uncertainties encompassing the spread from lowest 5% to highest 95%. For the Global_3
 480 group, the observational uncertainty is from Cowtan-Way, expanded by the spread of the three central
 481 estimates.
 482
 483
 484

<i>Series:</i>	<i>Period:</i>	1850-1900 to 2019	1850-1900 to 2010-2019	1880 - 2019	
		LOESS _{bsln}	Latest decade	LOESS _{md}	Linear
HadCRUT4		1.02 [0.93 - 1.11] (0.97 - 1.07)	0.93 (0.88 - 0.98)	0.99 [0.88 - 1.11] (0.94 - 1.04)	0.96 [0.82 - 1.10] (0.92 - 1.03)
NOAA GlobalTemp		1.09 [0.98 - 1.19]	0.99	1.06 [0.93 - 1.18]	1.04 [0.89 - 1.19]
NASA GISTEMP		1.12 [1.02 - 1.22]	1.01	1.09 [0.98 - 1.21]	1.04 [0.88 - 1.20]
Cowtan & Way		1.12 [1.04 - 1.21] (1.05 - 1.19)	1.01 (0.95 - 1.09)	1.14 [1.03 - 1.25] (1.08 - 1.21)	1.02 [0.88 - 1.15] (0.94 - 1.09)
Berkeley Earth		1.19 [1.10 - 1.27]	1.08	1.20 [1.09 - 1.31]	1.09 [0.96 - 1.22]
All Operational (OpAll)		1.11 [0.93 - 1.27]	1.00	1.10 [0.88 - 1.31]	1.03 [0.82 - 1.22]
Full Global (Global_3) *		1.14 * [1.02 - 1.27] (1.05 - 1.26)	1.03	1.14 [0.98 - 1.31]	1.05 [0.88 - 1.22]

485 For LOESS_{bsln} to 2019, there are minor differences in assessed values but no changes in dataset
 486 rankings versus LOESS_{md} 1880—2019. LOESS_{bsln} is generally ~0.1 °C higher than 1850—1900
 487 to 2010—2019 ΔGMST, reflecting the five-year offset and ~0.2 °C/decade recent warming
 488 (2010—2019 is centered at the end of 2014). At 1.14°C, Global_3 LOESS_{bsln} ΔGMST to 2019 is
 489 0.03°C higher than OpAll average, reflecting a 0.09°C difference with the mean of the two
 490 reduced coverage series from HadCRUT4 and NOAA GlobalTemp. The 1880—2019 LOESS_{md}
 491 discrepancy is even wider: 0.09°C for NOAA and 0.15°C for HadCRUT4. LOESS_{bsln} statistical
 492 fit uncertainties are smaller than LOESS_{md} or OLS, reflecting the smaller uncertainty of
 493 departure from the 1850—1900 mean rather than a single point (as noted in Section 2.2.2).



494
 495 **Figure 2: GMST series and group surface warming estimates.** (a) Monthly series and multi-decadal LOESS_{bsln}
 496 ΔGMST (span ± 20 years) are shown for HadCRUT4 (red), NOAA GlobalTemp (light blue), NASA GISTEMP
 497 (blue), Cowtan-Way (purple) and Berkeley Earth (orange), together with OLS and period estimates from IPCC AR5
 498 and SR15. NOAA GlobalTemp and NASA GISTEMP have been matched to the longer datasets over the

499 overlapping 1880—1900 period. Also shown are 24 CMIP6 SAT-SST model runs, blended following Cowtan et al
 500 (2015) and Richardson et al (2018). **(b)** LOESS_{bsln} (solid line with filled circle) is shown for two GMST groupings:
 501 Global_3 (purple) and OpAll (dark red). Also shown are selected additional warming estimates: anthropogenic
 502 following Hausteine et al (2017) (diamonds), decadal average (crosses) and OLS linear trend from 1880 (x-crosses).
 503 Recent IPCC Δ GMST estimates are highlighted by large squares: AR5 OLS to 2012 (light blue) and SR1.5 2006-
 504 2015 mean extended to 2017 (blue), together with corresponding Global_3 LOESS_{bsln} Δ GMST (purple).

505 The observation-based and CMIP6 blended ensemble LOESS_{bsln} (Figure 2a) show broadly
 506 similar changes: a rise to 1950, a 1950—1975 flattening, and strong post-1975 warming. The
 507 observations show stronger 1920—1950 warming, especially in the three HadSST-based series,
 508 and weaker post-1975 warming.

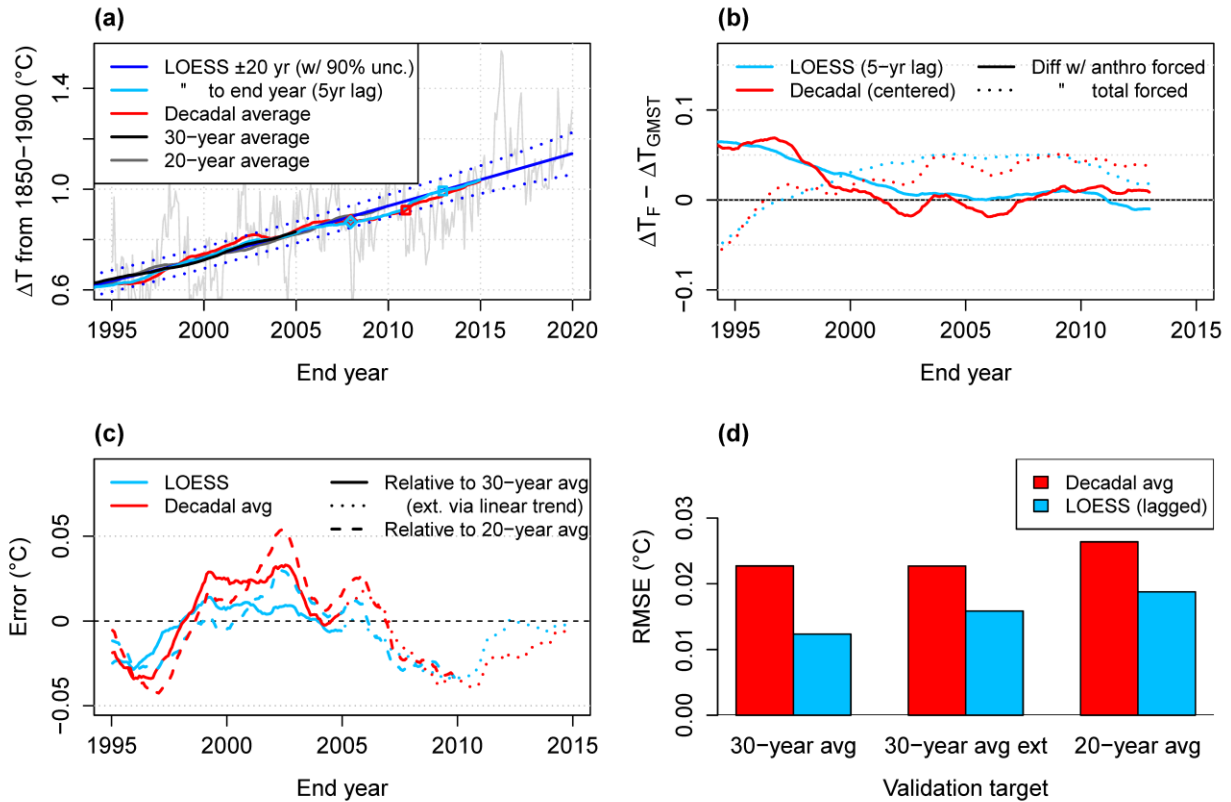
509 Separate tests showed that derived Δ GMST_{LOESS} was similar when restricting CMIP6 spatial
 510 coverage to that of Berkeley Earth, so we take the CMIP6 blended ensemble as directly
 511 comparable to the Global_3 series (Figure S14). The Global_3 rise of 1.14°C is just above the
 512 median CMIP6 estimate extended linearly to 2019, 1.12°C [0.91 – 1.41]. However, the Global_3
 513 current trend of 0.20°C/decade (as estimated by the LOESS_{bsln} slope at the 2019 end point) is
 514 lower than CMIP6’s 0.26°C/decade [0.18 – 0.38] or the likely ECS sub-ensemble’s
 515 0.25°C/decade [0.18 – 0.29].

516 In general, Figure 2(a) shows LOESS_{bsln} Δ GMST from the five updated observational datasets
 517 (coloured lines) are at or above recent IPCC long-term observational Δ GMST estimates
 518 (represented by crosses and x-crosses). Figure 2(b) affords a closer view of recent Δ GMST
 519 estimates, including group LOESS_{bsln} calculated to 2012 and 2017 for direct comparison to IPCC
 520 AR5 and SR1.5. As previously stated, AR5’s main estimate of 0.85°C was from linear OLS on
 521 the datasets available then. Since the mean 1880—2012 OLS trend for OpAll is 0.89°C and
 522 LOESS_{bsln} is 0.93°C, Δ GMST methodology accounts for half of the discrepancy between AR5’s
 523 1880—2012 estimate and our OpAll based estimate. The 2012 gap is even wider for the
 524 Global_3 group. OLS to 2012 is 0.90°C and LOESS_{bsln} is 0.96°C; that gap continues to grow,
 525 reaching 0.09°C in 2019.

526 The SR1.5 2006-2015 mean Δ GMST_{period} of 0.87°C, centered at the end of 2010, was extended
 527 to the most recent year (2017) to provide a then current estimate of 1.0°C (Section 1.2.1.3 in
 528 Allen et al., 2018). The same extension to 2017 applied to the updated series shows a 0.03°C gap
 529 with LOESS_{bsln} evaluated in 2017. This discrepancy may be related to internal variability
 530 suppressing early 2000s warming; the period difference estimate based on the most recent
 531 decade then available (2008-2017) shows no such discrepancy with LOESS_{bsln}. Both LOESS_{bsln}
 532 and period estimates are in good agreement with the slightly higher Hausteine human-induced
 533 warming Δ GMST_{F,anthro} estimates.

534 Figure 3 compares Global_3 LOESS_{bsln} and period Δ GMST in more detail. Since IPCC SR1.5
 535 explicitly considered the 2006-2015 mean as a proxy for the 1996-2025 average (relative to
 536 1850—1900), we consider the centered 20-year average and a 30-year “extended” average
 537 assuming the current linear 30-year trend continues over the next 15 years. We estimate that the
 538 1979—2019 warming has been approximately linear (see Table S2 showing OLS-LOESS
 539 agreement over this period), and the large ensembles also imply minor errors from assuming
 540 linearity through 2025. Figure 3a shows that in general LOESS_{bsln} departs less from the eventual
 541 20 and 30 year average than the decade mean and confirms that 2006-2015 was affected by an

542 early 2000s slowdown. LOESS_{bsln} has more stability relative to anthropogenic warming
 543 estimates (Figure 3b) with near-identical concordance with $\Delta\text{GMST}_{F,\text{anthro}}$ since 2003, and has
 544 lower RMSE relative to the longer period averages since the late 1990s (Figure 3c, 3d).



545
 546 **Figure 3: ΔGMST estimation method validation based on average of 3 global series.** (a) LOESS_{bsln} to 2019
 547 (blue) is shown with 5-year lagged LOESS (light blue), decadal average (red), 20-year average (light gray) and 30-
 548 year average (black). LOESS (light blue) versus decadal (red) differences are shown with (b) forced warming
 549 estimates following Haustein et al. (2017) and (c) validation targets (30-year average, 30-year average extended with
 550 linear trend and 20-year average). (d) RMSE is calculated from errors shown in (c).

551 The equivalent performance evaluation of long-term Global_3 LOESS_{bsln} versus OLS ΔGMST in
 552 Figure S15 shows a growing cool bias in OLS relative to the 20 and 30-year average from 1995
 553 on (Figure S15a) and thus much higher RMSE than LOESS_{bsln} relative to the longer period
 554 averages (Figure S15d).

555 Global_3 LOESS_{bsln} ΔGMST to 2019 is our main input for subsequent analysis such as
 556 remaining carbon budget, for which combined 17–83 % uncertainty is required; the combined
 557 statistical and observational uncertainty calculated following the method outlined in Section
 558 2.2.4 yields Global_3 ΔGMST of 1.14°C [1.05 – 1.25].

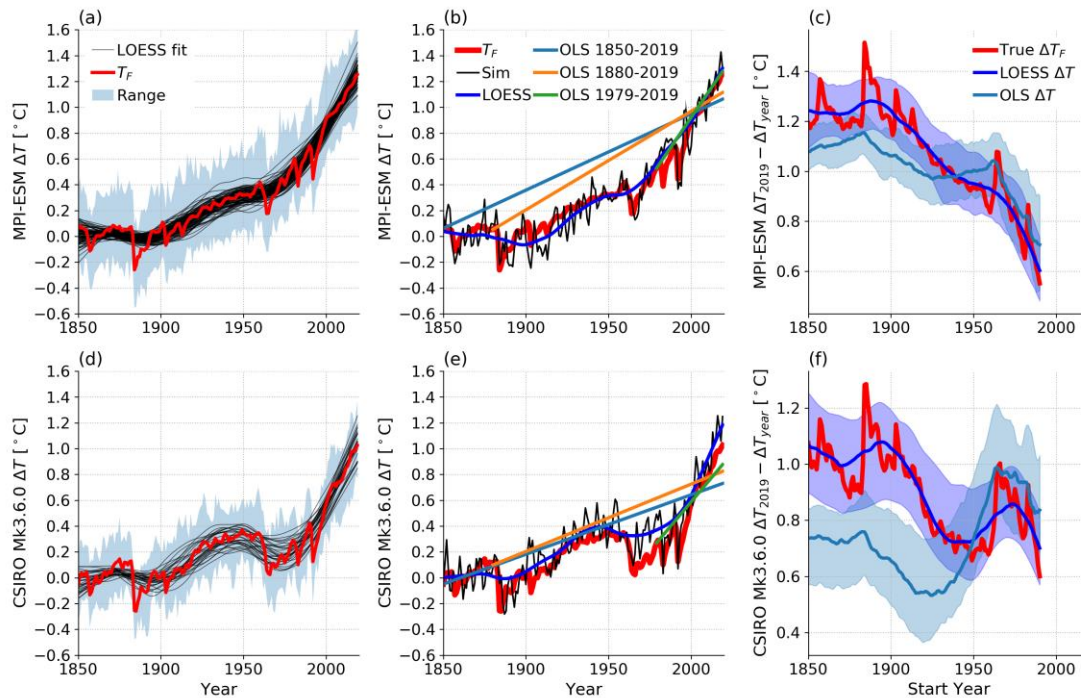
559 3.2 Large Ensemble Validation

560
 561 Figure 4(a,d) shows the MPI-GE and CSIRO Mk3.6.0 annual SAT range, individual LOESS_{md}
 562 fits and GSAT_F estimate, Figure 4(b,e) contains example LOESS and OLS fits to a single

563 simulation and Figure 4(c,f) shows the forced, LOESS and OLS ΔGSAT estimates through 2019
 564 for each start year from 1850—1980.

565 The ΔGSAT_F and LOESS ΔGSAT agree well outside of periodic ΔGSAT_F spikes from volcanic
 566 eruptions, i.e. when the forced change is smooth over our ± 20 year window, such that
 567 $\Delta\text{GSAT}_{\text{LOESS}} \approx \Delta\text{GSAT}_F$. For changes from the 19th century to recently, the IPCC AR5 estimates
 568 of solar forcing change are negligible compared with anthropogenic forcing so longer-term
 569 ΔGSAT_F should approximate the $\Delta\text{GSAT}_{F,\text{anthro}}$ used in our later carbon budget calculation.
 570 Meanwhile, OLS is biased relative to ΔGSAT_F in the long term, and is more sensitive to internal
 571 variability in the short term, e.g. for 1990—2019 OLS ensemble spread is 62 % (MPI-ESM) or
 572 26 % (CSIRO Mk3.6.0.) larger than LOESS ensemble spread.

573
 574



575
 576 **Figure 4.** (a) MPI-GE SAT outputs, full ensemble range is shaded, each simulation’s LOESS fit is in grey and the
 577 ensemble mean (our estimate of GSAT_F) is in red. (b) example of fits applied to a single simulation (black)
 578 including LOESS (dark blue) and OLS over three different periods (straight lines) with GSAT_F in red. OLS lines are
 579 shifted up so that their end points correspond to the relevant ΔGMST for ease of comparison. (c) calculated ΔGSAT
 580 for GSAT_F (red), based on the LOESS fit (dark blue) and based on OLS (cyan). For the fits, the lines are the
 581 ensemble median and the shaded regions the 5—95 % range. (d—f) as (a—c) but for the CSIRO Mk 3.6.0 ensemble.

582
 583 Table 3 contains the large ensemble ΔGSAT estimates. For periods like 1850—1900 to 2010—
 584 2019, we use Section 2.2.2’s $\text{LOESS}_{\text{bsln}}$ approach while OLS is fit between the middle of each
 585 period. In both ensembles LOESS performs similarly to the period difference with the 5th, 50th
 586 and 95th percentiles of the ensemble LOESS and period difference calculations all agreeing to
 587 within ≤ 0.02 $^{\circ}\text{C}$. LOESS slightly outperforms centered period differences evaluated from
 588 1850—1900 to end periods ranging from 1986—1995 through 2010—2019 when validated
 589 against 30-year average (see Figure S16). This validates LOESS performance, and Table 3

590 shows an advantage over period means since its calculation can be extended to the latest
 591 available year without greatly inflated uncertainty. The 0.06—0.10 °C discrepancies in the third
 592 column of Table 3 for 1880—2019 LOESS-GSAT_F are likely because the LOESS window
 593 centred at 1880 captures Krakatoa’s large post-1883 cooling, thereby reducing the 1880 LOESS
 594 estimate and increasing its 1880—2019 ΔGMST. These results show that such biases are period-
 595 dependent, are indeed negligible for 1850—1900 to 2019 in these models, and support our
 596 choice of time periods in the analysis using observational datasets.

597
 598 As our carbon budget calculations include an internal variability error component, we consider
 599 ensemble spread and statistical fit uncertainties as candidates and compare the LOESS_{bsln}
 600 ensemble 83rd minus 17th percentile and the statistical 17—83 % ranges for each run over 1850—
 601 1900 to 2019. The CSIRO Mk3.6.0 17—83 % ensemble spread in GSAT LOESS_{bsln} is 0.22 °C.
 602 This is larger than the median ensemble member’s statistical range (0.18 °C) and similar to the
 603 largest individual ensemble member range (0.22 °C). For MPI-ESM the ensemble spread (0.11
 604 °C) is smaller than the median statistical uncertainty (0.16 °C) and is marginally lower than the
 605 smallest member value (0.12 °C). For the internal variability component of ΔGSAT uncertainty
 606 in our carbon budgets we present results both using statistical uncertainty (derived only from
 607 observational data) and a more conservative estimate using the ±0.11 °C CSIRO Mk3.6.0
 608 ensemble spread.

609
 610 This large ensemble analysis has:

- 611 (i) provided limited support for our LOESS-based statistical uncertainty estimates
 612 being similar to model variability,
- 613 (ii) shown that LOESS matches or exceeds period difference performance while
 614 having lower long-term bias and short-term uncertainty than OLS,
- 615 (iii) verified that LOESS reliably reproduces ΔGSAT_F outside of years immediately
 616 following large volcanic eruptions, particularly supporting our LOESS_{bsln} results
 617 as an estimate of ΔGSAT_{F,anthro}.

618
 619
 620 **Table 3. Long-term ΔGSAT estimated for various periods for the ensemble mean T_F, plus the ensemble**
 621 **medians and 5—95 % ranges for estimates based on LOESS, OLS or taking the mean of the raw SAT**
 622 **outputs. Uncertainties in T_F differences are derived by treating T_F as a sample mean and assuming the**
 623 **ensemble members follow a Gaussian distribution in any given year. The period errors are then combined in**
 624 **quadrature.**

	MPI-ESM ΔGSAT[°C] median [5—95 %] [17—83 %]		
Method	1850-1900 to 2010-2019	1850-1900 to 2019	1880 to 2019
T _F	1.15 [1.15-1.16] [1.15-1.16]	1.25 [1.23-1.28] [1.24-1.27]	1.20 [1.17-1.23] [1.18-1.22]
LOESS	1.16 [1.07-1.24] [1.11-1.21]	1.25 [1.15-1.36] [1.21-1.32]	1.26 [1.15-1.36] [1.20-1.31]
OLS	1.02 [0.93-1.12] [0.97-1.07]	1.13 [1.04-1.23] [1.08-1.18]	1.15 [1.06-1.23] [1.10-1.20]
Individual runs	1.15 [1.07-1.24] [1.11-1.20]	1.24 [1.04-1.48] [1.12-1.40]	1.20 [0.92-1.50] [1.04-1.39]
	CSIRO Mk3.6.0 ΔGMST[°C]		
T _F	0.92 [0.90-0.93] [0.91-0.92]	1.03 [0.99-1.07] [1.00-1.05]	0.93 [0.88-0.98] [0.90-0.96]
LOESS	0.93 [0.79-1.04] [0.82-1.01]	1.05 [0.89-1.18] [0.90-1.12]	1.03 [0.84-1.16] [0.91-1.10]

OLS	0.63 [0.46-0.72] [0.52-0.70]	0.73 [0.56-0.85] [0.61-0.82]	0.75 [0.58-0.87] [0.64-0.83]
Individual runs	0.91 [0.78-1.04] [0.83-1.00]	1.03 [0.81-1.22] [0.86-1.12]	0.94 [0.66-1.15] [0.76-1.05]

625

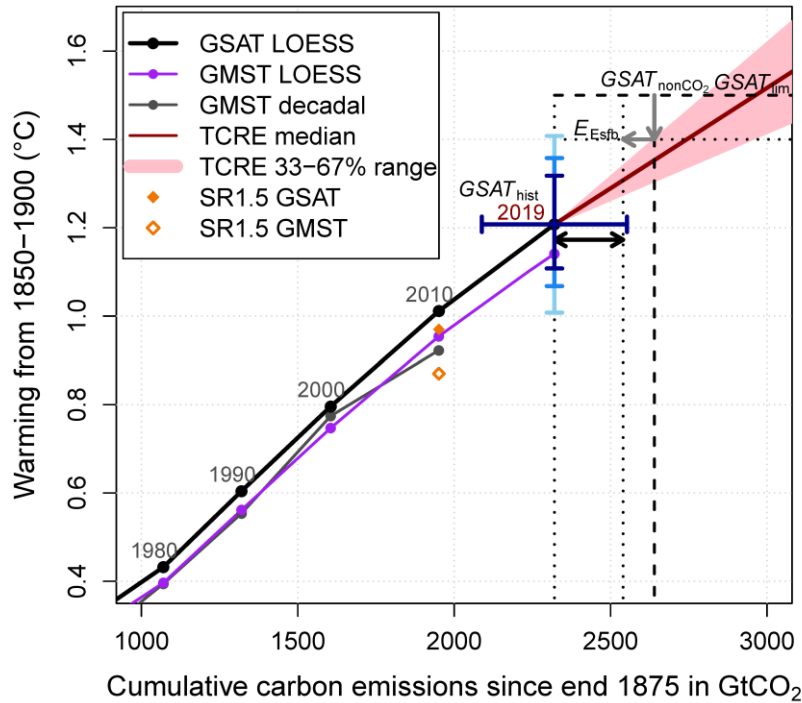
626

3.3 Global SAT Estimate and Remaining Carbon Budget

627 We now convert our best estimate $\Delta\text{GMST}_{\text{LOESS}}$ of 1.14°C [$1.05 - 1.25$] (17—83% uncertainty)
 628 to an equivalent $\Delta\text{GSAT}_{\text{LOESS}}$ as outlined in Section 2.2.4. Our CMIP6 ensemble $\text{LOESS}_{\text{bsln}}$
 629 A_{blend} ratio $\Delta\text{GSAT}_{\text{LOESS}}/\Delta\text{GMST}_{\text{LOESS}}$ reflects an increase of $\Delta\text{GSAT}_{\text{LOESS}}$ over full-coverage
 630 $\Delta\text{GMST}_{\text{LOESS}}$ of 5.8% [4.4, 7.2] in 2014, i.e. long-term near-surface air temperature warming is
 631 5.8% greater than our blended estimate. This A_{blend} estimate is very similar to equivalent CMIP5-
 632 based estimates, but much lower than the 24% derived in CMIP5 for 1861—1880 to 2006—2015
 633 using a HadCRUT4-like masking and blending algorithm (Richardson et al., 2016). This is due
 634 to the different handling of sea ice and the incorporation of complete (unadjusted) spatial
 635 coverage in the A_{blend} calculation.

636 Combining this ratio and its uncertainty with our Global_3 $\Delta\text{GMST}_{\text{LOESS}}$, as outlined in Section
 637 2.2.4, we obtain $\Delta\text{GSAT}_{\text{LOESS}}$ of 1.21°C [$1.11 - 1.32$] from 1850—1900 to 2019, a lower
 638 uncertainty than the equivalent SR1.5 estimate of $\pm 0.12^{\circ}\text{C}$ (Section 1.2.1.2 in Allen et al., 2018).
 639 The conservative CSIRO-based internal variability yields a wider $\Delta\text{GSAT}_{\text{LOESS}}$ range of $1.07 -$
 640 1.37°C . These estimates all represent uncertainty in total forced warming; however, uncertainty
 641 in anthropogenic warming was estimated to be still higher at $\pm 0.2^{\circ}\text{C}$ (Section 1.2.1.3 in Allen et
 642 al., 2018). The equivalent $\text{LOESS}_{\text{bsln}}$ HadCRUT4 estimate using the SR1.5 correction of ~15%
 643 yields slightly lower $\Delta\text{GSAT}_{\text{obs}}$ of 1.17°C , and the updated SR1.5 2006—2015 estimate extended
 644 to end of 2019 is 1.15°C . Finally, A_{blend} corrected $\text{LOESS}_{\text{bsln}}$ HadCRUT4 yields 1.08°C ; the
 645 difference of 0.13°C with our main $\Delta\text{GSAT}_{\text{LOESS}}$ primarily reflects HadCRUT4 coverage bias, as
 646 well as a small sea ice edge effect. The other carbon budget calculation components also have
 647 large uncertainties. Cumulative emissions to end of 2019 are $2320 \pm 230 \text{ GtCO}_2$ (Friedlengstein
 648 et al., 2019), while non- CO_2 uncertainties are even higher (see Table 2.2 in Rogelj et al., 2018).
 649 Although no formal methods exist to combine these uncertainties, Rogelj et al (2018) estimated
 650 overall uncertainty of $\pm 50\%$ in SR1.5 remaining carbon budgets.

651 Figure 5 shows the calculation for the remaining carbon budget with a 66% chance to stay below
 652 1.5°C , along with the historical cumulative CO_2 emissions and temperature change.



653

654

655 **Figure 5: Global temperature change from 1850–1900 versus cumulative CO₂ emissions.** The smoothed
 656 temperature response from the Global3 blended GMST group as decadal average (blue) and LOESS_{bsln} trend
 657 (purple) are shown relative to cumulative CO₂ emissions from Friedlingsten et al (2019). The thick black line shows
 658 the Global3 GSAT LOESS_{bsln} trend, obtained by adjusting GMST by the ratio of GSAT and blended GMST
 659 historical runs from an ensemble of 24 CMIP5 models. The pink shaded plume and dark red line are estimated
 660 temperature response to cumulative CO₂ emissions (TCRE) from the beginning of 2020 on. Also shown are other
 661 remaining carbon budget factors, T_{nonCO_2} and E_{Esfb} (gray arrows). The thick black double arrow represents the
 662 remaining carbon budget for 66% chance of remaining below 1.5°C. Vertical error bars show ΔGSAT combined
 663 observational and statistical uncertainty (dark blue), combined observational and internal variability derived from
 664 CSIRO ensemble (medium blue) and estimated uncertainty in anthropogenic warming (light blue).

665 Our remaining carbon budgets incorporate the SR1.5 Table 2.2 100 GtCO₂ adjustment for earth-
 666 system feedbacks (CO₂ and CH₄ release from warming wetland and permafrost thaw), following
 667 recent practice established in Rogelj et al. (2019) and Nauels et al. (2019). Carbon budgets
 668 excluding this term are therefore 100 GtCO₂ higher, as in the SR1.5 “headline” remaining carbon
 669 budget of 420 GtCO₂ (IPCC, 2018) to remain under 1.5°C (with 66% chance).

670 The remaining carbon budgets from the start of 2020 for a 66% (50%) chance to stay below
 671 1.5°C and 2.0°C are 220 (350) GtCO₂ and 880 (1270) GtCO₂ respectively (rounded to nearest 5
 672 GtCO₂). Given current annual emissions of just over 40 GtCO₂, the 66% 1.5°C remaining carbon
 673 budget is only ~15 GtCO₂ lower than the equivalent carbon budgets including earth-system
 674 feedbacks in SR1.5 Table 2.2 (320 GtCO₂ from 2018) and Nauels et al (235 GtCO₂ from 2020).

675 However, our 50% 1.5°C carbon budget is ~45 GtCO₂ below those two studies. This follows
 676 from the slightly higher $\Delta\text{GSAT}_{\text{obs}}$ found in this study, combined with an identical TCRE spread
 677 starting in 2020 rather than the SR1.5 reference period centered at the start of 2011. In effect, the
 678 up-to-date LOESS_{bsln} estimate of $\Delta\text{GSAT}_{\text{obs}}$ reduces the contribution of TCRE uncertainty, as
 679 there is less ΔT “to go”.

680 SR1.5’s secondary carbon budgets used the average ΔGMST through 2006—2015 to obtain a 66
 681 % chance of staying below 1.5 °C resulting in an equivalent budget of 470 GtCO₂ from 2018
 682 (i.e. 385 GtCO₂ from 2020). Our alternative budget using Global_3 $\Delta\text{GMST}_{\text{LOESS}}$ instead of
 683 $\Delta\text{GSAT}_{\text{LOESS}}$ is 305 GtCO₂ from 2020. This large difference relative to SR1.5 is unsurprising as
 684 the Global_3 series show more historical warming whereas the SR1.5 $\Delta\text{GMST}_{\text{period}}$ average
 685 included HadCRUT4 and its more substantial coverage bias. We also note that an OLS 1880—
 686 2019 ΔGMST basis would imply even higher 1.5 °C 66% remaining carbon budgets of 455
 687 GtCO₂ (Global_3) or 485 (GtCO₂ (OpAll)).

688 **4 Discussion and Conclusions**

689 We have explored the range of warming estimates since the late 19th century across different
 690 observational series using multiple estimation methodologies, focusing on the Global_3 subset of
 691 extensively interpolated datasets (NASA GISTEMP, Cowtan-Way and Berkeley Earth). Our
 692 main LOESS_{bsln} Global_3 ΔGMST since 1850—1900 is, to our knowledge, the first such
 693 estimator that (i) integrates robust statistical uncertainties, with fit residuals following the
 694 assumed noise process, (ii) has been extended to provide a corresponding $\Delta\text{GSAT}_{\text{LOESS}}$ since
 695 1850—1900, including combined observational and internal variability uncertainties, and (iii)
 696 has been validated against output from model large ensembles.

697 IPCC SR1.5 reported $\Delta\text{GMST}_{\text{period}}$ of 0.87°C to 2006—2015 using four datasets (1.0°C when
 698 extended to 2017) and estimated $\Delta\text{GSAT}_{\text{period}}$ of 0.97°C by adjusting one dataset (HadCRUT4)
 699 for biases related to incomplete coverage and sea-air temperature differences, effectively
 700 discarding the other three. The ensuing carbon budget calculation included cumulative emissions
 701 up to 2017, necessitating an implicit extension of $\Delta\text{GSAT}_{\text{period}}$ to that date. The simplicity and
 702 coherence of our “up-to-date” $\Delta\text{GMST}_{\text{LOESS}}$ and $\Delta\text{GSAT}_{\text{LOESS}}$ estimates represent a clear
 703 advance over the IPCC ΔGMST period difference and ΔGSAT derivation methods. Not only is
 704 LOESS_{bsln} generally an unbiased $\Delta\text{GMST}_{\text{F}}$ estimator outside periods of volcanism, but the
 705 method includes a more consistent and intuitive baseline alignment of datasets beginning in 1880
 706 and maintains the previously stated advantage of including statistical uncertainty derived using a
 707 noise model consistent with the data. Moreover, validation tests with observations and the large
 708 ensembles confirm LOESS_{bsln} results in lower biases relative to $\Delta\text{GSAT}_{\text{F}}$ and lower
 709 susceptibility to natural variation. None of this is surprising considering that the IPCC period
 710 difference method is essentially a 10-year moving average.

711 Another key difference with IPCC SR1.5 is our consistent use of the Global_3 datasets with
 712 extensive spatial interpolation. As previously noted in section 2.1.1, these datasets are
 713 demonstrably more representative of global climate change and require smaller and less
 714 uncertain adjustments (~6%) to obtain $\Delta\text{GSAT}_{\text{LOESS}}$ from $\Delta\text{GMST}_{\text{LOESS}}$, in contrast to the 15%
 715 adjustment applied to HadCRUT4 $\Delta\text{GMST}_{\text{period}}$ in IPCC SR1.5. The Global_3 datasets give 0.12

716 °C more warming than HadCRUT4 from 1850—1900 and the divergence related to unmitigated
 717 bias coverage may well grow, as the Global_3 LOESS_{md} trend is now 0.03°C/decade higher than
 718 HadCRUT4’s 0.17 °C/decade. Focusing on the three Global_3 datasets and our robust LOESS_{bsln}
 719 estimator dramatically reduces the spread between Δ GMST estimates: the inter-dataset spread in
 720 Global_3 LOESS_{bsln} 1850—1900 to 2019 Δ GMST is only 0.07°C. Including the non-global
 721 datasets increases the LOESS_{bsln} spread to 0.17 °C, and including OLS and LOESS_{md} trend
 722 methodologies increases the spread to 0.27 °C: from 0.93°C (OLS for HadCRUT4) to 1.20°C
 723 (Berkeley Earth LOESS_{md}).

724 SR1.5 also reported 1880—2012 and 1880—2015 linear trend Δ GMST, but mainly to provide
 725 “traceability” to the IPCC AR5. In contrast, AR5’s main estimate of 0.85°C was based on the
 726 mean linear trend of available datasets, while HadCRUT4 2003—2012 period difference from
 727 1850—1900 Δ GMST estimate was a primary input for further analyses such as future projections
 728 (Collins et al., 2013) and attribution (Bindoff et al., 2013).

729 If IPCC AR6 follows AR5 and provides both period difference and point-to-point trends for
 730 datasets beginning in 1850, that would imply the three post-1850 datasets would form the basis
 731 for 2010—2019 period Δ GMST_{obs} relative to 1850—1900. As noted above though, LOESS_{bsln} to
 732 2019 offers a superior alternative. Since HadCRUT4 clearly does not meet our “quasi-global”
 733 criterion, we omit it as a direct component of Δ GMST_{LOESS}. Nevertheless, HadCRUT4 and its
 734 underlying land and ocean datasets (CRUTEM4 and HadSST3) form the essential basis of
 735 Cowtan-Way, and HadSST3 is also a key component of Berkeley Earth. Following the precedent
 736 set in IPCC SR1.5, the ERSSTv5 based datasets starting 1880 should also be considered, using
 737 baseline matching over 1880—1900. Our Global_3 group member, NASA GISTEMP is an
 738 obvious choice for inclusion, while NOAA GlobalTemp could be omitted according to our
 739 global coverage criterion. However, that case is less clear cut than HadCRUT4 due to NOAA’s
 740 complicated spatial coverage. Once again, though, NOAA’s GHCNv4 and ERSSTv5 datasets
 741 would still be present as they form the essential basis of NASA GISTEMP.

742 The recent release of HadCRUT5 (Morice et al., 2020) will certainly inform future regular
 743 updates of our main Δ GMST_{LOESS} and Δ GSAT_{LOESS} estimates. HadCRUT5 features sophisticated
 744 kriging interpolation, resulting in virtual coverage similar to Berkeley Earth, and incorporates
 745 updated datasets for land (CRUTEM5; Osborn et al., 2020) and ocean (HadSST4; Kennedy et
 746 al., 2019). We give a preliminary evaluation of the eventual effect of HadCRUT5 (and
 747 HadSST4) in Table S4. The incorporation of HadSST4 (instead of HadSST3) into Cowtan-Way
 748 and Berkeley Earth results in a noticeable increase in Δ GMST_{LOESS}, while results for
 749 HadCRUT5 are nearly identical to Cowtan-Way/HadSST4.

750 Since observational datasets beginning in 1880, such as NASA GISTEMP, potentially could be
 751 included alongside the three datasets starting in 1850, LOESS_{bsln} Δ GMST arguably renders
 752 1880—2019 Δ GMST_{OLS} redundant in IPCC AR6. However, AR5 also compared long-term
 753 Δ GMST_{OLS} trends starting from 1880 to short-term trends starting from mid-century or later. Our
 754 results reinforce that 1880—2019 linear trend is inconsistent with LOESS_{md} 1880—2019
 755 Δ GMST. The bias of long-term OLS Δ GMST was confirmed in analysis of two large ensembles,
 756 which also showed that it has 26—62 % larger uncertainty than LOESS_{md} for recent 30-year
 757 trends. As seen in Table S2, observed OLS trends from 1951 have wider uncertainty than the

758 corresponding LOESS_{md} estimates and show evidence of warm bias as well (for example the
 759 NASA GISTEMP 1951—2019 OLS is almost identical to 1880—2019). We therefore
 760 recommend LOESS_{md} over linear trend for both long-term (> 120 years) and short-term (30-70
 761 years) intervals.

762 LOESS_{bsln} statistical uncertainties represent another opportunity for AR6. If $\Delta\text{GMST}_{\text{LOESS}}$ is
 763 close enough to $\Delta\text{GMST}_{\text{F}}$ then with an appropriate noise model the $\Delta\text{GMST}_{\text{LOESS}}$ uncertainty due
 764 to internal variability could be derived from the LOESS residuals. We combined this with
 765 observational uncertainty and carried it forward directly to $\Delta\text{GSAT}_{\text{LOESS}}$ for carbon budget
 766 calculations, but it could also be used for other follow-on analyses. The median statistical
 767 uncertainties from the large ensemble runs are within 25% of the ensemble spreads, and the
 768 residual autocorrelation structure implies potential for this approach.

769 However, global climate models may not capture long-term internal variability (Brown et al.,
 770 2015). For example, recent Pacific changes may indicate stronger real-world multi-decadal
 771 variability (e.g. England et al., 2014), although consensus is lacking (Seager et al., 2019). We
 772 take no position on the ability of models to generate this variability, only note that it has been
 773 studied in CMIP5 (e.g. Brown et al., 2015) and CMIP6 (e.g. Parsons et al., 2020) and report on
 774 how errors would affect our conclusions. Substantial internal variability on ± 20 year timescales
 775 or longer would result in underestimated LOESS uncertainties. By contrast, large forced changes
 776 on shorter timescales, such as due to volcanism, would increase the uncertainties. Nevertheless,
 777 our method derives uncertainties directly from observations and so may have advantages over
 778 approaches that rely on model outputs or estimated forcings (Otto et al 2015; Hausteine et al.,
 779 2017).

780 Given the above caveats we provided a more conservative ΔGSAT uncertainty incorporating the
 781 CSIRO model large ensemble spread and its pronounced internal variability. Since our
 782 $\Delta\text{GMST}_{\text{LOESS}}$ and $\Delta\text{GSAT}_{\text{LOESS}}$ estimates are close to observation-based anthropogenic warming,
 783 confirming a basic finding of IPCC SR1.5, we treat our $\Delta\text{GSAT}_{\text{LOESS}}$ as an estimate of
 784 $\Delta\text{GSAT}_{\text{F,anthro}}$, albeit with appropriately wider uncertainties. In general, our approach yields
 785 straightforward and up-to-date estimates of ΔGMST and ΔGSAT to inform remaining carbon
 786 budget calculations that incorporate appropriate ΔGSAT uncertainties .

787 To summarize, we argue strongly in favor of LOESS_{bsln} ΔGMST using series with near-global
 788 coverage. Combining our statistical estimate of internal variability with dataset spread and
 789 dataset parametric uncertainty results in a best estimate of warming from 1850—1900 to 2019 of
 790 1.14 °C [1.05 – 1.25] (17-83% uncertainty). Not only is this updated through 2019, rather than
 791 the prior-decade value of the IPCC’s period mean difference, but it includes a potentially useful
 792 statistical fit uncertainty that is not readily or typically derived for period mean differences.

793 Our CMIP6-derived GSAT adjustment yields corresponding $\Delta\text{GSAT}_{\text{LOESS}}$ of 1.21°C [1.11–1.32]
 794 (17—83% uncertainty), implying a remaining carbon budget of ~220 GtCO₂ for a 66% chance
 795 that ΔGSAT since 1850—1900 remains below 1.5°C. This carbon budget is ~5.5 years of current
 796 emissions and is less than half the 455–485 GtCO₂ carbon budget implied by an OLS ΔGMST
 797 basis. Our ΔGSAT estimate uncertainty can be adapted to a desired interpretation of ΔGSAT , for
 798 example, as total or anthropogenic warming. All $\Delta\text{GSAT}_{\text{LOESS}}$ and $\Delta\text{GMST}_{\text{LOESS}}$ indices can be

799 updated annually and are only dependent on the temperature datasets, yielding a set of
800 transparent and easily communicated metrics to measure progress towards climate goals.

801

802

803 **Acknowledgments and Data**

804 The authors thank Andrew Dessler for provision of MPI-GE series. DCC thanks Shaun Lovejoy
805 and Lenin Del Rio Amador for clarifying discussions.

806 MR's contribution was carried out at the Jet Propulsion Laboratory, California Institute of
807 Technology under a contract with the National Aeronautics and Space Administration
808 (80NM0018D004).

809 Berkeley Earth data are available from <http://berkeleyearth.org/data/>. Cowtan-Way data,
810 including merged HadSST4 series, are available from [http://www-](http://www-users.york.ac.uk/~kdc3/papers/coverage2013/series.html)
811 [users.york.ac.uk/~kdc3/papers/coverage2013/series.html](http://www-users.york.ac.uk/~kdc3/papers/coverage2013/series.html). HadCRUT4.6 data are available from
812 <https://www.metoffice.gov.uk/hadobs/hadcrut4/data/current/download.html>. HadCRUT5 data are
813 available from <https://www.metoffice.gov.uk/hadobs/hadcrut5/data/current/download.html>.
814 NASA GISTEMP data are available from <https://data.giss.nasa.gov/gistemp/>. NOAA
815 GlobalTemp data are available from [https://www.ncei.noaa.gov/data/noaa-global-surface-](https://www.ncei.noaa.gov/data/noaa-global-surface-temperature/v5/access/timeseries/)
816 [temperature/v5/access/timeseries/](https://www.ncei.noaa.gov/data/noaa-global-surface-temperature/v5/access/timeseries/). CMIP6 data are available from [https://esgf-](https://esgf-node.llnl.gov/search/cmip6/)
817 [node.llnl.gov/search/cmip6/](https://esgf-node.llnl.gov/search/cmip6/).

818

819 **References**

- 820 Allen, M.R., Dube, O.P., Solecki, W., Aragón-Durand, F., Cramer, W., Humphreys, S.,
821 Kainuma, M., et al. (2018). Framing and Context. In V. Masson-Delmotte, et al. (Eds.), *Global*
822 *Warming of 1.5°C: An IPCC Special Report on the impacts of global warming of 1.5°C above*
823 *pre-industrial levels and related global greenhouse gas emission pathways, in the context of*
824 *strengthening the global response to the threat of climate change, sustainable development, and*
825 *efforts to eradicate poverty*. Intergovernmental Panel on Climate Change.
- 826 Bindoff, N.L., Stott, P.A., AchutaRao, K.M., Allen, M.R., Gillett, N., et al., 2013: Detection and
827 Attribution of Climate Change: from Global to Regional. In: *Climate Change 2013: The Physical*
828 *Science Basis*. Contribution of Working Group I to the Fifth Assessment Report of the
829 Intergovernmental Panel on Climate Change [Stocker, T.F., Qin, D., Plattner, G.-K., Tignor, M.,
830 Allen, S.K., et al. (Eds.)]. Cambridge University Press, Cambridge, United Kingdom and New
831 York, NY, USA.
- 832 Brohan, P., Kennedy, J. J., Harris, I., Tett, S. F. B., & Jones, P. D. (2006). Uncertainty estimates
833 in regional and global observed temperature changes: A new data set from 1850. *Journal of*
834 *Geophysical Research*, 111(D12). <https://doi.org/10.1029/2005jd006548>
- 835 Brown, P. T., Li, W., & Xie, S.-P. (2015). Regions of significant influence on unforced global
836 mean surface air temperature variability in climate models. *Journal of Geophysical Research:*
837 *Atmospheres*, 120(2), 480–494. <https://doi.org/10.1002/2014jd022576>

- 838 Cahill, N., Rahmstorf, S., & Parnell, A. C. (2015). Change points of global temperature.
 839 *Environmental Research Letters*, 10(8), 84002. <https://doi.org/10.1088/1748-9326/10/8/084002>
- 840 Cleveland, W. S. (1979). Robust Locally Weighted Regression and Smoothing Scatterplots.
 841 *Journal of the American Statistical Association*, 74(368), 829–836.
 842 <https://doi.org/10.1080/01621459.1979.10481038>
- 843 Cleveland, W. S., & Grosse, E. (1991). Computational methods for local regression. *Statistics*
 844 *and Computing*, 1(1), 47–62. <https://doi.org/10.1007/bf01890836>
- 845 Cleveland, W. S., Grosse, E., & Shyu, W. M. (1991), Local regression models. In J.M.
 846 Chambers, & T. Hastie (Eds.), *Statistical Models in S*, Wadsworth, Pacific Grove, Calif.
- 847 Collins M, et al. (2013) Long-term Climate Change: Projections, Commitments and
 848 Irreversibility. In: *Climate Change 2013: The Physical Science Basis. Contribution of Working*
 849 *Group I to the Fifth Assessment Report of the Intergovernmental Panel on Climate Change*, eds
 850 Stocker TF, et al. (Cambridge University Press, Cambridge, United Kingdom and New York,
 851 NY, USA).
- 852 Cowtan, K., Hausfather, Z., Hawkins, E., Jacobs, P., Mann, M. E., Miller, S. K., et al. (2015).
 853 Robust comparison of climate models with observations using blended land air and ocean sea
 854 surface temperatures. *Geophysical Research Letters*, 42(15), 6526–6534.
 855 <https://doi.org/10.1002/2015GL064888>
- 856 Cowtan, K., Jacobs, P., Thorne, P., & Wilkinson, R. (2018a). Statistical analysis of coverage
 857 error in simple global temperature estimators. *Dynamics and Statistics of the Climate System*,
 858 3(1). <https://doi.org/10.1093/climsys/dzy003>
- 859 Cowtan, K., Rohde, R., & Hausfather, Z. (2018b). Evaluating biases in sea surface temperature
 860 records using coastal weather stations. *Quarterly Journal of the Royal Meteorological Society*,
 861 144(712), 670–681. <https://doi.org/10.1002/qj.3235>
- 862 Cowtan, K., & Way, R. G. (2014a). Coverage bias in the HadCRUT4 temperature series and its
 863 impact on recent temperature trends. *Quarterly Journal of the Royal Meteorological Society*,
 864 140(683), 1935–1944. <https://doi.org/10.1002/qj.2297>
- 865 Cowtan, K., & Way, R. G. (2014b). Update to “Coverage bias in the HadCRUT4 temperature
 866 series and its impact on recent temperature trends”. *Temperature reconstruction by domain:*
 867 *version 2.0 temperature series*. <https://doi.org/10.13140/RG.2.1.4728.0727>
- 868 Deser, C., Lehner, F., Rodgers, K. B., Ault, T., Delworth, T. L., DiNezio, P. N., et al. (2020).
 869 Insights from Earth system model initial-condition large ensembles and future prospects. *Nature*
 870 *Climate Change*, 10(4), 277–286. <https://doi.org/10.1038/s41558-020-0731-2>
- 871 Dessler, A. E., Mauritsen, T., & Stevens, B. (2018). The influence of internal variability on
 872 Earth’s energy balance framework and implications for estimating climate sensitivity.
 873 *Atmospheric Chemistry and Physics*, 18(7), 5147–5155. [https://doi.org/10.5194/acp-18-5147-](https://doi.org/10.5194/acp-18-5147-2018)
 874 2018

- 875 England, M. H., McGregor, S., Spence, P., Meehl, G. A., Timmermann, A., Cai, W., et al.
 876 (2014). Recent intensification of wind-driven circulation in the Pacific and the ongoing warming
 877 hiatus. *Nature Climate Change*, 4(3), 222–227. <https://doi.org/10.1038/nclimate2106>
- 878 Eyring, V., Bony, S., Meehl, G. A., Senior, C. A., Stevens, B., Stouffer, R. J., & Taylor, K. E.
 879 (2016). Overview of the Coupled Model Intercomparison Project Phase 6 (CMIP6) experimental
 880 design and organization. *Geoscientific Model Development*, 9(5), 1937–1958.
 881 <https://doi.org/10.5194/gmd-9-1937-2016>
- 882 Flato, G., Marotzke, J., Abiodun, B., Braconnot, P., Chou, S.C., et al. (2013). Evaluation of
 883 Climate Models. In: *Climate Change 2013: The Physical Science Basis. Contribution of Working*
 884 *Group I to the Fifth Assessment Report of the Intergovernmental Panel on Climate Change*
 885 [Stocker, T.F., Qin, D., Plattner, G.-K., Tignor, M., Allen, S.K., et al. (Eds.)]. Cambridge
 886 University Press, Cambridge, United Kingdom and New York, NY, USA.
- 887 Forster, P. M., Maycock, A. C., McKenna, C. M., & Smith, C. J. (2019). Latest climate models
 888 confirm need for urgent mitigation. *Nature Climate Change*. [https://doi.org/10.1038/s41558-019-](https://doi.org/10.1038/s41558-019-0660-0)
 889 [0660-0](https://doi.org/10.1038/s41558-019-0660-0)
- 890 Foster, G., & Rahmstorf, S. (2011). Global temperature evolution 1979–2010, *Environmental*
 891 *Research Letters*, 6(4), 44022. <https://doi.org/10.1088/1748-9326/6/4/044022>
- 892 Freeman, E., Woodruff, S. D., Worley, S. J., Lubker, S. J., Kent, E. C., Angel, W. E., et al.
 893 (2016). ICOADS Release 3.0: a major update to the historical marine climate record.
 894 *International Journal of Climatology*, 37(5), 2211–2232. <https://doi.org/10.1002/joc.4775>
- 895 Friedlingstein, P., Jones, M. W., O., Sullivan, M., Andrew, R. M., Hauck, J., Peters, G. P., et al.
 896 (2019). Global Carbon Budget 2019. *Earth System Science Data*, 11(4), 1783–1838.
 897 <https://doi.org/10.5194/essd-11-1783-2019>
- 898 Goodwin, P., Katavouta, A., Roussenov, V. M., Foster, G. L., Rohling, E. J., & Williams, R. G.
 899 (2018). Pathways to 1.5 °C and 2 °C warming based on observational and geological constraints.
 900 *Nature Geoscience*, 11(2), 102–107. <https://doi.org/10.1038/s41561-017-0054-8>
- 901 Hansen, J., Sato, M., Ruedy, R., Lo, K., Lea, D. W., & Medina-Elizade, M. (2006). Global
 902 temperature change. *Proceedings of the National Academy of Sciences*, 103(39), 14288–14293.
 903 <https://doi.org/10.1073/pnas.0606291103>
- 904 Hansen, J., Ruedy, R., Sato, M., Imhoff, M., Lawrence, W., Easterling, D., et al. (2001). A closer
 905 look at United States and global surface temperature change. *Journal of Geophysical Research:*
 906 *Atmospheres*, 106(D20), 23947–23963. <https://doi.org/10.1029/2001jd000354>
- 907 Hartmann, D.L., A.M.G. Klein Tank, M. Rusticucci, L.V. Alexander, S. Brönnimann, et al.,
 908 2013a: Observations: Atmosphere and Surface. In: *Climate Change 2013: The Physical Science*
 909 *Basis. Contribution of Working Group I to the Fifth Assessment Report of the Intergovernmental*
 910 *Panel on Climate Change* [Stocker, T.F., Qin, D., Plattner, G.-K., Tignor, M., Allen, S.K., et al.
 911 (Eds.)]. Cambridge University Press, Cambridge, United Kingdom and New York, NY, USA.

- 912 Hartmann, D.L., A.M.G. Klein Tank, M. Rusticucci, L. Alexander, S. Brönnimann, et al.
 913 (2013b): Observations: Atmosphere and Surface Supplementary Material. In: Climate Change
 914 2013: The Physical Science Basis. Contribution of Working Group I to the Fifth Assessment
 915 Report of the Intergovernmental Panel on Climate Change [Stocker, T.F., Qin, D., Plattner, G.-
 916 K., Tignor, M., Allen, S.K., et al. (Eds.)]. Cambridge University Press, Cambridge, United
 917 Kingdom and New York, NY, USA.
- 918 Hausfather, Z., Cowtan, K., Clarke, D. C., Jacobs, P., Richardson, M., & Rohde, R. (2017).
 919 Assessing recent warming using instrumentally homogeneous sea surface temperature records.
 920 *Science Advances*, 3(1), e1601207. <https://doi.org/10.1126/sciadv.1601207>.
- 921 Haustein, K., Allen, M. R., Forster, P. M., Otto, F. E. L., Mitchell, D. M., Matthews, H. D., &
 922 Frame, D. J. (2017). A real-time Global Warming Index. *Scientific Reports*, 7(1).
 923 <https://doi.org/10.1038/s41598-017-14828-5>
- 924 Hawkins, E., Burt, S., Brohan, P., Lockwood, M., Richardson, H., Roy, M., & Thomas, S.
 925 (2019). Hourly weather observations from the Scottish Highlands (1883–1904) rescued by
 926 volunteer citizen scientists. *Geoscience Data Journal*, 6(2), 160–173.
 927 <https://doi.org/10.1002/gdj3.79>
- 928 Hoegh-Guldberg, O., Jacob, D., Taylor, M., Bindi, M., Brown, S., et al., 2018: Impacts of 1.5°C
 929 Global Warming on Natural and Human Systems. Global Warming of 1.5°C. An IPCC Special
 930 Report on the impacts of global warming of 1.5°C above pre-industrial levels and related global
 931 greenhouse gas emission pathways, in the context of strengthening the global response to the
 932 threat of climate change, sustainable development, and efforts to eradicate poverty [Masson-
 933 Delmotte, V., P. Zhai, H.-O. Pörtner, D. Roberts, J. Skea, P.R. Shukla, et al. (eds.)].
- 934 Huang, B., Thorne, P. W., Banzon, V. F., Boyer, T., Chepurin, G., Lawrimore, J. H., et al.
 935 (2017). Extended Reconstructed Sea Surface Temperature, Version 5 (ERSSTv5): Upgrades,
 936 Validations, and Intercomparisons. *Journal of Climate*, 30(20), 8179–8205.
 937 <https://doi.org/10.1175/jcli-d-16-0836.1>
- 938 Huang, B., Menne, M. J., Boyer, T., Freeman, E., Gleason, B. E., Lawrimore, J. H., et al. (2020).
 939 Uncertainty Estimates for Sea Surface Temperature and Land Surface Air Temperature in
 940 NOAA GlobalTemp Version 5. *Journal of Climate*, 33(4), 1351–1379.
 941 <https://doi.org/10.1175/jcli-d-19-0395.1>
- 942 IPCC, 2013: Summary for Policymakers. In Climate Change 2013: The Physical Science Basis.
 943 Contribution of Working Group I to the Fifth Assessment Report of the Intergovernmental Panel
 944 on Climate Change [Stocker, T.F., Qin, D., Plattner, G.-K., Tignor, M., Allen, S.K., et al. (Eds.)].
 945 Cambridge University Press, Cambridge, United Kingdom and New York, NY, USA.
- 946 IPCC, 2014: Climate Change 2014: Synthesis Report. Contribution of Working Groups I, II and
 947 III to the Fifth Assessment Report of the Intergovernmental Panel on Climate Change [Core
 948 Writing Team, R.K. Pachauri and L.A. Meyer (eds.)]. IPCC, Geneva, Switzerland.
- 949 IPCC, 2013: Summary for Policymakers. In Global Warming of 1.5°C. An IPCC Special Report
 950 on the impacts of global warming of 1.5°C above pre-industrial levels and related global

- 951 greenhouse gas emission pathways, in the context of strengthening the global response to the
 952 threat of climate change, sustainable development, and efforts to eradicate poverty [Masson-
 953 Delmotte, V., Zhai, P., Pörtner, H.-O., Roberts, D., Skea, J., Shukla, P.R., Pirani, A., et al.
 954 (eds.)]. World Meteorological Organization, Geneva, Switzerland, 32 pp.
- 955 Jeffrey, S. J., Rotstayn, L. D., Collier, M. A., Dravitzki, S. M., Hamalainen, C., Moeseneder, C.,
 956 Wong, K. K., & Syktus, J. I. (2013). Australia's CMIP5 submission using the CSIRO Mk3.6
 957 model, *Australian Meteorological and Oceanographic Journal*, 63, 1–13,
 958 http://www.bom.gov.au/amoj/docs/2013/jeffrey_hres.pdf
- 959 Jones, P. D., Lister, D. H., Osborn, T. J., Harpham, C., Salmon, M., & Morice, C. P. (2012).
 960 Hemispheric and large-scale land-surface air temperature variations: An extensive revision and
 961 an update to 2010. *Journal of Geophysical Research: Atmospheres*, 117(D5), n/a-n/a.
 962 <https://doi.org/10.1029/2011jd017139>
- 963 Karl, T. R., Arguez, A., Huang, B., Lawrimore, J. H., McMahon, J. R., Menne, M. J., et al.
 964 (2015). Possible artifacts of data biases in the recent global surface warming hiatus. *Science*,
 965 348(6242), 1469–1472. <https://doi.org/10.1126/science.aaa5632>
- 966 Kennedy, J. J., Rayner, N. A., Atkinson, C. P., & Killick, R. E. (2019). An Ensemble Data Set of
 967 Sea Surface Temperature Change From 1850: The Met Office Hadley Centre HadSST.4.0.0.0
 968 Data Set. *Journal of Geophysical Research: Atmospheres*, 124(14), 7719–7763.
 969 <https://doi.org/10.1029/2018jd029867>
- 970 Kennedy, J. J., Rayner, N. A., Smith, R. O., Parker, D. E., & Saunby, M. (2011). Reassessing
 971 biases and other uncertainties in sea surface temperature observations measured in situ since
 972 1850: 1. Measurement and sampling uncertainties. *Journal of Geophysical Research*, 116(D14).
 973 <https://doi.org/10.1029/2010jd015218>
- 974 Kennedy, J. J., Rayner, N. A., Smith, R. O., Parker, D. E., & Saunby, M. (2011). Reassessing
 975 biases and other uncertainties in sea surface temperature observations measured in situ since
 976 1850: 2. Biases and homogenization. *Journal of Geophysical Research*, 116(D14).
 977 <https://doi.org/10.1029/2010jd015220>
- 978 Lenssen, N. J. L., Schmidt, G. A., Hansen, J. E., Menne, M. J., Persin, A., Ruedy, R., & Zyss, D.
 979 (2019). Improvements in the GISTEMP Uncertainty Model. *Journal of Geophysical Research:*
 980 *Atmospheres*, 124(12), 6307–6326. <https://doi.org/10.1029/2018JD02952>.
- 981 Maher, N., Milinski, S., Suarez-Gutierrez, L., Botzet, M., Dobrynin, M., Kornbluh, L., et al.
 982 (2019). The Max Planck Institute Grand Ensemble: Enabling the Exploration of Climate System
 983 Variability. *Journal of Advances in Modeling Earth Systems*, 11(7), 2050–2069.
 984 <https://doi.org/10.1029/2019ms001639>
- 985 Menne, M. J., Williams, C. N., Gleason, B. E., Rennie, J. J., & Lawrimore, J. H. (2018). The
 986 Global Historical Climatology Network Monthly Temperature Dataset, Version 4. *Journal of*
 987 *Climate*, 31(24), 9835–9854. <https://doi.org/10.1175/jcli-d-18-0094.1>

- 988 Morice, C. P., Kennedy, J. J., Rayner, N. A., & Jones, P. D. (2012). Quantifying uncertainties in
 989 global and regional temperature change using an ensemble of observational estimates: The
 990 HadCRUT4 data set. *Journal of Geophysical Research: Atmospheres*, 117(D8).
 991 <https://doi.org/10.1029/2011jd017187>
- 992 Morice, C. P., Kennedy, J. J., Rayner, N. A., Winn, J. P., Hogan, E., Killick, R. E., et al. (2020).
 993 An updated assessment of near-surface temperature change from 1850: the HadCRUT5 dataset,
 994 submitted to *Journal of Geophysical Research: Atmospheres*, in review
- 995 Mudelsee, M. (2019). Trend analysis of climate time series: A review of methods. *Earth-Science*
 996 *Reviews*, 190, 310–322. <https://doi.org/10.1016/j.earscirev.2018.12.005>
- 997 Nauels, A., Rosen, D., Mauritsen, T., Maycock, A., McKenna, C., Roegli, J., et al. (2019). ZERO
 998 IN ON the remaining carbon budget and decadal warming rates. The CONSTRAIN Project
 999 Annual Report 2019. University of Leeds. <https://doi.org/10.5518/100/20>
- 1000 Nychka, D., Buchberger, R., Wigley, T. M. L., Santer, B. D., Taylor, K. E., & Jones, R. (2000).
 1001 Confidence intervals for trend estimates with autocorrelated observations. NCAR manuscript.
 1002 <https://opensky.ucar.edu/islandora/object/manuscripts:881>
- 1003 Osborn, T.J., Jones, P.D., Lister, D.H., Morice, C.P., Simpson, I.R, Winn, J, , et al . (2020). Land
 1004 surface air temperature variations across the globe updated to 2019: the CRUTEM5 dataset.
 1005 *Journal of Geophysical Research*, accepted.
- 1006 Parsons, L. A., Brennan, M. K., Wills, R. C. J., & Proistosescu, C. (2020). Magnitudes and
 1007 Spatial Patterns of Interdecadal Temperature Variability in CMIP6. *Geophysical Research*
 1008 *Letters*, 47(7). <https://doi.org/10.1029/2019gl086588>
- 1009 Peng-Fei, L., F. Xiao-Li, & L. Juan-Juan (2015), Historical Trends in Surface Air Temperature
 1010 Estimated by Ensemble Empirical Mode Decomposition and Least Squares Linear Fitting,
 1011 *Atmospheric and Oceanic Science Letters*: 8:1, 10-16. <https://doi.org/10.3878/AOSL20140064>
- 1012 Rahmstorf, S., Foster, G., & Cahill, N. (2017). Global temperature evolution: recent trends and
 1013 some pitfalls. *Environmental Research Letters*, 12(5), 54001. <https://doi.org/10.1088/1748-9326/aa6825>
 1014
- 1015 Richardson, M., Cowtan, K., & Millar, R. J. (2018). Global temperature definition affects
 1016 achievement of long-term climate goals. *Environmental Research Letters*, 13(5), 54004.
 1017 <https://doi.org/10.1088/1748-9326/aab305>
- 1018 Rogelj, J., Shindell, D., Jiang, K., Fifita, S., Forster, P., Ginzburg, V., et al., 2018: Mitigation
 1019 Pathways Compatible with 1.5°C in the Context of Sustainable Development. In: *Global*
 1020 *Warming of 1.5°C. An IPCC Special Report on the impacts of global warming of 1.5°C above*
 1021 *pre-industrial levels and related global greenhouse gas emission pathways, in the context of*
 1022 *strengthening the global response to the threat of climate change, sustainable development, and*
 1023 *efforts to eradicate poverty [Masson-Delmotte, V., P. Zhai, H.-O. Pörtner, D. Roberts, J. Skea,*
 1024 *P.R. Shukla, et al. (eds.)].*

- 1025 Rogelj, J., Forster, P. M., Kriegler, E., Smith, C. J., & Séférian, R. (2019). Estimating and
 1026 tracking the remaining carbon budget for stringent climate targets. *Nature*, 571(7765), 335–342.
 1027 <https://doi.org/10.1038/s41586-019-1368-z>
- 1028 Risbey, J. S., Lewandowsky, S., Cowtan, K., Oreskes, N., Rahmstorf, S., Jokimäki, A., & Foster,
 1029 G. (2018). A fluctuation in surface temperature in historical context: reassessment and
 1030 retrospective on the evidence. *Environmental Research Letters*, 13(12), 123008.
 1031 <https://doi.org/10.1088/1748-9326/aaf342>
- 1032 Rohde, R. A., & Hausfather, Z. (2020). The Berkeley Earth Land/Ocean Temperature Record.
 1033 *Earth System Science Data*, 12(4), 3469–3479. <https://doi.org/10.5194/essd-12-3469-2020>
- 1034 Rohde, R., Muller, R.A., Jacobsen, R., Muller, E., Perlmutter, C., et al. (2013). A New Estimate
 1035 of the Average Earth Surface Land Temperature Spanning 1753 to 2011. *Geoinformatics &*
 1036 *Geostatistics: An Overview*, 1(1). <https://doi.org/10.4172/2327-4581.1000101>
- 1037 Rotstayn, L. D., Jeffrey, S. J., Collier, M. A., Dravitzki, S. M., Hirst, A. C., Syktus, J. I., &
 1038 Wong, K. K. (2012). Aerosol- and greenhouse gas-induced changes in summer rainfall and
 1039 circulation in the Australasian region: a study using single-forcing climate simulations.
 1040 *Atmospheric Chemistry and Physics*, 12(14), 6377–6404. [https://doi.org/10.5194/acp-12-6377-](https://doi.org/10.5194/acp-12-6377-2012)
 1041 [2012](https://doi.org/10.5194/acp-12-6377-2012)
- 1042 Santer, B. D., Thorne, P. W., Haimberger, L., Taylor, K. E., Wigley, T. M. L., Lanzante, J. R., et
 1043 al. (2008). Consistency of modelled and observed temperature trends in the tropical troposphere.
 1044 *International Journal of Climatology*, 28(13), 1703–1722. <https://doi.org/10.1002/joc.1756>
- 1045 Seager, R., Cane, M., Henderson, N., Lee, D.-E., Abernathey, R., & Zhang, H. (2019).
 1046 Strengthening tropical Pacific zonal sea surface temperature gradient consistent with rising
 1047 greenhouse gases. *Nature Climate Change*, 9(7), 517–522. [https://doi.org/10.1038/s41558-019-](https://doi.org/10.1038/s41558-019-0505-x)
 1048 [0505-x](https://doi.org/10.1038/s41558-019-0505-x)
- 1049 Smith, T.M., and R.W. Reynolds, 2005: A global merged land and sea surface temperature
 1050 reconstruction based on historical observations (1880–1997). *J. Clim.*, 18, 2021–2036
- 1051 Susskind, J., Schmidt, G. A., Lee, J. N., & Iredell, L. (2019). Recent global warming as
 1052 confirmed by AIRS. *Environmental Research Letters*, 14(4), 44030.
 1053 <https://doi.org/10.1088/1748-9326/aafd4e>
- 1054 Trenberth, K.E., Jones, P.D., Ambenje, P., Bojariu, R., Easterling, D., et al., 2007: Observations:
 1055 Surface and Atmospheric Climate Change. In: *Climate Change 2007: The Physical Science*
 1056 *Basis. Contribution of Working Group I to the Fourth Assessment Report of the*
 1057 *Intergovernmental Panel on Climate Change* [Solomon, S., Qin, D., Manning, M., Chen, Z.,
 1058 Marquis, M., et al. (eds.)]. Cambridge University Press, Cambridge, United Kingdom and New
 1059 York, NY, USA.
- 1060 UNFCCC, 2015, Report on the Structured Expert Dialogue on the 2013–2015 Review
 1061 FCCC/SB/2015/INF.1

- 1062 Takahashi, H., Lebsock, M. D., Richardson, M., Marchand, R., & Kay, J. E. (2019). When Will
1063 Spaceborne Cloud Radar Detect Upward Shifts in Cloud Heights? *Journal of Geophysical*
1064 *Research: Atmospheres*. <https://doi.org/10.1029/2018jd030242>
- 1065 van den Dool, H. M., Saha, S., & Johansson, Å. (2000). Empirical Orthogonal Teleconnections.
1066 *Journal of Climate*, 13(8), 1421–1435. [https://doi.org/10.1175/1520-](https://doi.org/10.1175/1520-0442(2000)013<1421:eot>2.0.co;2)
1067 [0442\(2000\)013<1421:eot>2.0.co;2](https://doi.org/10.1175/1520-0442(2000)013<1421:eot>2.0.co;2)
- 1068 Visser, H., Dangendorf, S., van Vuuren, D. P., Bregman, B., & Petersen, A. C. (2018). Signal
1069 detection in global mean temperatures after “Paris”: an uncertainty and sensitivity analysis.
1070 *Climate of the Past*, 14(2), 139–155. <https://doi.org/10.5194/cp-14-139-2018>
- 1071 Zhang, H.-M., Lawrimore, J., Huang, B., Menne, M., Yin, X., Sanchez-Lugo, A., Gleason, B.E.,
1072 et al. (2019). Updated Temperature Data Give a Sharper View of Climate Trends. *Eos*, 100.
1073 <https://doi.org/10.1029/2019eo128229>
- 1074 **(c) 2021. All Rights Reserved**